A TWO-DIMENSIONAL "FLEA ON THE ELEPHANT" PHENOMENON AND ITS NUMERICAL VISUALIZATION

Roberta Bianchini, Laurent Gosse, Enrique Zuazua

A TWO-DIMENSIONAL "FLEA ON THE ELEPHANT" PHENOMENON AND ITS NUMERICAL VISUALIZATION

ROBERTA BIANCHINI*, LAURENT GOSSE†, AND ENRIQUE ZUAZUA‡

Abstract. Localization phenomena (sometimes called "*flea on the elephant*") for the operator $L^\varepsilon = -\varepsilon^2\Delta u + p(\mathbf{x})u$, $p(\mathbf{x})$ being an asymmetric double-well potential, are studied both analytically and numerically, mostly in two space dimensions within a perturbative framework. Starting from a classical harmonic potential, the effects of various perturbations are retrieved, especially in the case of two asymmetric potential wells. These findings are illustrated numerically by means of an original algorithm, which relies on a discrete approximation of the Steklov-Poincaré operator for L^ε, and for which error estimates are established. Such a two-dimensional discretization produces less mesh-imprinting than more standard finite-differences and captures correctly sharp layers.

Key words. Asymmetric double-well potential; Lipschitz domains; Schrödinger equation;

AMS subject classifications. 35P20, 35Q40, 65N06, 65N15.

1. Introduction and preliminaries.

The "flea on the elephant" is an expression coined by Barry Simon in [47] to describe the following counter-intuitive phenomenon: being $V(x,y)$ a symmetric (smooth) two-well potential and $V+\delta V$ an arbitrarily small (smooth) perturbation of it, then for $0<\varepsilon\ll 1$, corresponding perturbed eigenfunctions will preferably localize in the largest well (see also [38]).

1.1. Elementary "flea on the elephant" in 1D.

Given $\varepsilon>0$, we start from the steady one-dimensional Schrödinger equation for some energy level E_ε,

$$-\varepsilon\partial_{xx}\psi_\varepsilon + V(x)\psi_\varepsilon = E_\varepsilon\,\psi_\varepsilon(x), \qquad x\in(0,1),$$

where, for $0<a<b<1$, the (square-wells) potential $V(x)$ is piecewise constant,

$$V(x) = \bar V\chi_{x\in(a,b)} + \infty\Big(\chi_{x<0}+\chi_{x>1}\Big), \qquad \bar V>0.$$

Dirichlet conditions correspond to infinite potential walls: $\psi(0)=\psi(1)=0$,

$$k := k(E_\varepsilon) = \sqrt{\frac{E_\varepsilon}{\varepsilon}}, \qquad \kappa := \kappa(E_\varepsilon) = \sqrt{\frac{\bar V - E_\varepsilon}{\varepsilon}},$$

describe bound-states, so that,

$$\forall x\in(0,1), \quad \psi(x) = \begin{cases} A\sin kx, & x\in(0,a)\\ B\exp(\kappa(x-a)) + C\exp(\kappa(b-x)), & \\ D\sin k(1-x), & x\in(b,1),\end{cases}$$

where (real) constants A,B,C,D are such that C^1 smoothness holds:

$$\left[\begin{array}{rcl} A\sin ka &=& B + C\exp(\kappa(b-a))\\ D\sin k(1-b) &=& B\exp(\kappa(b-a)) + C\end{array}\right\} \ C^0 \text{ smoothness},$$
$$\left[\begin{array}{rcl} kA\cos ka &=& \kappa[B - C\exp(\kappa(b-a))]\\ -kD\cos k(1-b) &=& \kappa[B\exp(\kappa(b-a)) - C]\end{array}\right\} \ C^1 \text{ smoothness}, \tag{1.1}$$

*Unité de mathématiques pures et appliquées, École normale supérieure de Lyon, 46, allée d'Italie 69364 Lyon Cedex 07 (France). roberta.bianchini@ens-lyon.fr

†IAC–CNR "Mauro Picone", Via dei Taurini 19, 00185 Rome (Italy) l.gosse@ba.iac.cnr.it

‡DeustoTech, University of Deusto, 48007 Bilbao, Basque Country (Spain), Departamento de Matemáticas, Universidad Autónoma de Madrid, 28049 Madrid, (Spain). enrique.zuazua@deusto.es

The vector of coefficients can be characterized by means of the kernel of a 4×4 matrix,

$$\begin{vmatrix} \sin ka & -1 & -\exp(\kappa(b-a)) & 0 \\ 0 & -\exp(\kappa(b-a)) & -1 & \sin k(1-b) \\ \frac{k}{\kappa}\cos ka & -1 & \exp(\kappa(b-a)) & 0 \\ 0 & \exp(\kappa(b-a)) & -1 & \frac{k}{\kappa}\cos k(1-b) \end{vmatrix} = 0.$$

Since (1.1) implies,

$$\frac{A(\kappa\sin ka + k\cos ka)}{D(\kappa\sin k(1-b) - k\cos k(1-b))} = \exp(\kappa(a-b)),$$
$$\frac{A(\kappa\sin ka - k\cos ka)}{D(\kappa\sin k(1-b) + k\cos k(1-b))} = \exp(\kappa(b-a)),$$

then

$$\boxed{\frac{A^2\cos^2 ka(\kappa^2\tan^2 ka - k^2)}{D^2\cos^2 k(1-b)(\kappa^2\tan^2 k(1-b) - k^2)} = 1,} \tag{1.2}$$

so that, when $a = 1-b$ in (1.2), symmetry, $D^2 = A^2$, easily follows. The asymmetric case is less straightforward in terms of algebra, even in 1D, see for instance [20, 31, 38, 45, 49] and [26, Chapter 2]. Accordingly, numerical simulations of a 1D explicit example are displayed in Fig. 1.1. Finite-differences based on $\mathcal{L}$-splines and borrowed

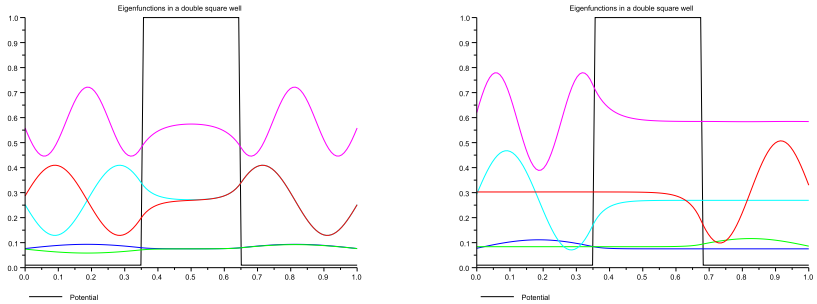

FIGURE 1.1. *Eigenfunctions for symmetric (left) vs. asymmetric (right) square wells.*

from [18] were set up in order to maximize both stability and accuracy in this context of a square-well potential: namely, we implemented both,

$$a = 0.35, b = 0.65 \text{ on the left,} \qquad a = 0.35, b = 0.675 \text{ on the right,}$$

with $\varepsilon = 0.001$, 2^7 grid points, and the following discretization,

$$r_{j\pm\frac{1}{2}} = \sqrt{\frac{V(x_{j\pm\frac{1}{2}})}{\varepsilon}}, \qquad -\frac{\varepsilon}{\Delta x}\left[\frac{r_{j+\frac{1}{2}}}{\sinh(r_{j+\frac{1}{2}}\Delta x)}\left(\psi_{j+1} - \cosh(r_{j+\frac{1}{2}}\Delta x)\psi_j\right)\right.$$
$$\left. - \frac{r_{j-\frac{1}{2}}}{\sinh(r_{j-\frac{1}{2}}\Delta x)}\left(\cosh(r_{j-\frac{1}{2}}\Delta x)\psi_j - \psi_{j-1}\right)\right] = E_\varepsilon\psi_j.$$

The (Anderson-like) localization process [14] is easy to see; similar behavior occurs in 2D, too, as shown in Fig. 5.5 for two symmetric, and asymmetric, Gaussian well potentials. Heuristically, it is explained by recalling that the curvature of eigenfunctions grows with their energy: the widest well (lying at the same depth) allows the ground state to have a larger wavelength, hence a smaller curvature. This kind of strong Accumulation phenomenon due to any little perturbation is known in literature as "the flea on the elephant", with a complete analysis given in [7, 32, 39, 44, 48].

1.2. Plan of the paper. In several dimensions, the spectral effects of perturbing a quadratic potential were studied in the literature, see for instance [32, 27, 47, 48, 30]. In those papers, from both a mathematical physics and a functional analysis perspective, many results were stated; there are also other probabilistic approaches in this direction, with applications to large deviations, see [46] and more recent references quoted in [30]. Accordingly, in Section 2, basic results for the harmonic potential are derived, so that, in Section 3, perturbations can be studied, especially concerning the width of the wells and their location. Section 4 deals with a 2D extension of the "$\mathcal{L}$-spline scheme" set up in 1D: its derivation follows [17] and is presented in §4.1 and some error estimates are given in §4.3. Section 5 contains some computational results, mostly for the accuracy on the harmonic potential in a square domain, and for perturbations of a two-well potential. Concluding remarks are given in Section 6, where the ability of the 2D scheme to capture sharp layers is illustrated in Fig. 6.1. Appendix A recalls regularity results for elliptic equations in square domains, following either [8, 21, 29] or [2, 28, 34, 24] for a study of "compatibility conditions".

2. Gaussian eigenfunctions of the quadratic potential. Let a differential operator $L^\varepsilon(u) := -\varepsilon^2\Delta u + p(\mathbf{x})u$ have a potential with conditions [P]:

- $p(\mathbf{x}) \in C^2(\mathbb{R}^N)$, $p(\mathbf{x}) \geq 0$;
- $p(\mathbf{x})$ has exactly two quadratic minima located in $\mathbf{x}_i$, for $i = 1, 2$

$$\lim_{\mathbf{x}\to\mathbf{x}_i} \frac{p(\mathbf{x})}{|\mathbf{x}-\mathbf{x}_i|^2} = C_i, \text{ for some constants } C_i.$$

More general potentials were considered in, *e.g.*, [7, 26, 39, 44]. In the whole space $\mathbf{x} \in \mathbb{R}^N$, the eigenvalue problem for the harmonic oscillator reads,

$$p(\mathbf{x}) = \frac{N}{2} + \frac{|\mathbf{x}|^2}{4\varepsilon^2}, \qquad L^\varepsilon(u) = -\varepsilon^2\Delta u + \left(\frac{N}{2} + \frac{|\mathbf{x}|^2}{4\varepsilon^2}\right) u, \tag{2.1}$$

being $|\cdot|$ the Euclidean norm. Inserting a change of variables,

$$\forall \mathbf{x} \in \mathbb{R}^N, \qquad u(\mathbf{x}) := \exp\left(\frac{|\mathbf{x}|^2}{4\varepsilon^2}\right) w(\mathbf{x}) \quad \text{inside} \quad L^\varepsilon(u) = \lambda u, \tag{2.2}$$

yields a (steady) convection-diffusion equation,

$$\tilde{L}^\varepsilon(w) := \exp\left(-\frac{|\mathbf{x}|^2}{4\varepsilon^2}\right) L^\varepsilon(u) = \big(-\varepsilon^2\Delta w - \mathbf{x}\cdot\nabla w\big) = \lambda w. \tag{2.3}$$

Namely, in terms of the new variable $w(\mathbf{x})$, the spectral problem (2.1) reads

$$-\varepsilon^2\Delta w(\mathbf{x}) - \mathbf{x}\cdot\nabla w(\mathbf{x}) = \lambda w(\mathbf{x}), \qquad \mathbf{x} \in \mathbb{R}^N. \tag{2.4}$$

Convection-diffusion problem (2.4) recasts as a drift-diffusion (conservative) one,

$$-\varepsilon^2\nabla\cdot(K^\varepsilon(x)\nabla w)-\lambda w K^\varepsilon(x)=0,\qquad K^\varepsilon(\mathbf{x})=\exp\left(\frac{|\mathbf{x}|^2}{2\varepsilon^2}\right), \tag{2.5}$$

so that nontrivial solutions to (2.4) are critical points of the following functional:

$$f\mapsto E_\varepsilon(f)=\frac{\varepsilon^2}{2}\int_{\mathbb{R}^N}|\nabla f|^2K^\varepsilon(\mathbf{x})\,\mathrm{d}\mathbf{x}-\frac{\lambda}{2}\int_{\mathbb{R}^N}|f(\mathbf{x})|^2K^\varepsilon(\mathbf{x})\,\mathrm{d}\mathbf{x}, \tag{2.6}$$

for f belonging, for ε fixed, to the following "weighted Sobolev space",

$$H^1(K^\varepsilon)=\left\{f:\mathbb{R}^N\to\mathbb{R}:\int_{\mathbb{R}^N}\left(|f|^2+\varepsilon^2|\nabla f|^2\right)K^\varepsilon(\mathbf{x})\,\mathrm{d}\mathbf{x}<+\infty\right\}. \tag{2.7}$$

Proposition 1. *For $K^\varepsilon(x)$ being as in (2.5) and $H^1(K^\varepsilon)$ given by (2.7), the continuous embedding $H^1(K^\varepsilon)\subset L^2(K^\varepsilon)$ is compact,*

$$H^1(K^\varepsilon)\subset\subset L^2(K^\varepsilon):=\left\{f:\mathbb{R}^N\to\mathbb{R}:\int_{\mathbb{R}^N}|f|^2K^\varepsilon(x)\,dx<+\infty\right\}.$$

Proof. The proof contained in [13] applies, based on the following lemma:

Lemma 1. *For any $f\in C_c^1(\mathbb{R}^N)$, the Poincaré inequality holds:*

$$\int_{\mathbb{R}^N}|f|^2\left(\frac{N}{2}+\frac{|\mathbf{x}|^2}{4\varepsilon^2}\right)K^\varepsilon(\mathbf{x})\,\mathrm{d}\mathbf{x}\le\varepsilon^2\int_{\mathbb{R}^N}|\nabla f|^2K^\varepsilon(\mathbf{x})\,\mathrm{d}\mathbf{x}. \tag{2.8}$$

□

The differential operator $\tilde{L}^\varepsilon$ in (2.3) is set in the domain

$$D(\tilde{L}^\varepsilon)=\left\{f\in H^1(K^\varepsilon);\,\tilde{L}^\varepsilon f\in L^2(K^\varepsilon)\right\}:=H^2(K^\varepsilon), \tag{2.9}$$

in which it is self-adjoint and, by Proposition 1, $D(\tilde{L}^\varepsilon)\subset\subset L^2(K^\varepsilon)$ compactly embedded. This implies that $\tilde{L}^\varepsilon$ presents an increasing sequence of eigenvalues $(\lambda_k)_{k\ge0}$, where $\lambda_0>0$ is guaranteed by inequality (2.8). Moreover, for any $m\ge0$,

$$\text{if}\quad f\in L^2(K^\varepsilon),\quad\text{then}\quad(1+|\xi|^2)^{\frac{m}{2}}\hat{f}\in L^2(\mathbb{R}^N),$$

so that the Fourier transform $\hat{f}$ is smooth,

$$\forall m\ge0,\qquad\hat{f}\in H^m(\mathbb{R}^N),\qquad\hat{f}\in C^\infty(\mathbb{R}^N).$$

It remains to take the Fourier transform of (2.4),

$$\varepsilon^2|\xi|^2\hat{w}(\xi)+N\hat{w}(\xi)+\xi\cdot\nabla\hat{w}(\xi)=\lambda\hat{w}(\xi),\qquad\widehat{(x_j\partial_{x_j}w)}(\xi)=-\hat{w}(\xi)-\xi_j\partial_{\xi_j}\hat{w}(\xi). \tag{2.10}$$

Another change of variables yields,

$$\xi\cdot\nabla v(\xi)=(\lambda-N)v(\xi),\qquad v(\xi)=\exp(\varepsilon^2\frac{|\xi|^2}{2})\hat{w}(\xi),$$

thus, $v(\xi)$ is a polynomial function of degree $(\lambda-N)=k-1$, $k\in\mathbb{N}$, namely

$$v(\xi)=P_{k-1}(\xi),\qquad P_{k-1}(\xi)\qquad\text{homogeneous polynomial of degree } k-1,$$

and solutions to (2.10) satisfy $\hat{w}(\xi) = \exp(-\varepsilon^2|\xi|^2/2)P_{k-1}(\xi)$, see also [13].

THEOREM 2.1. *The eigenvalues of $\tilde{L}^\varepsilon$ in (2.3), where $D(\tilde{L}^\varepsilon) \subset\subset H^1(K^\varepsilon)$, are*

$$\lambda_k = N + k - 1, \quad k \in \mathbb{N}, \tag{2.11}$$

with the ground-state and its related eigenfunctions,

$$\phi_0^\varepsilon(\mathbf{x}) := \exp\left(-\frac{|\mathbf{x}|^2}{2\varepsilon^2}\right), \qquad D^\alpha\phi_0^\varepsilon(\mathbf{x}), \quad \alpha = (\alpha_1, \cdots, \alpha_N),\ |\alpha| = k-1.$$

3. Perturbation analysis of the two wells potential. Hereafter, double well potentials with identical and different wells are considered, in order to show the role played by symmetry. In the symmetric case with $\varepsilon \ll 1$, eigenfunctions accumulate equally in both wells; oppositely, for asymmetric potentials, the ground state fills mostly the widest well (see [30] for more of a differential geometry approach). We qualitatively analyze effects of symmetry breaking in the potential shape $p(\mathbf{x})$:

- accumulation of solutions in the widest well;
- the role played by the position of the perturbation;
- how a perturbation affects the spectrum of the original problem.

Consider the spectral problem associated with

$$D(L^\varepsilon) \ni u \mapsto L^\varepsilon(u) = -\varepsilon^2\Delta u + \frac{p(\mathbf{x})}{4\varepsilon^2}u, \quad \text{where } p(\mathbf{x}) \text{ satifies [P]}, \tag{3.1}$$

the following statements hold true:

- the ground state accumulates in the widest well;
- potential perturbations' affect the spectral problem as much as they are close to the wells;
- eigenvalues and eigenfunctions' modifications occur according to the way the perturbation acts on the eigenfunctions of the original spectral problem.

3.1. Accumulation in the widest well. Yet, pick $0 < \varepsilon \ll 1$, and consider the spectral problem (3.1), mostly when $p(\mathbf{x})$ is a $C^2(\mathbb{R}^N)$ has two wells at the same height but with possibly different widths. Its eigenvalues form an increasing sequence, whose minimum λ_1 is given by Rayleigh's quotient,

$$\lambda_1 = \inf_{u \in D(L^\varepsilon)} \frac{\int_{\mathbb{R}^N} \varepsilon^2|\nabla u|^2 + \frac{p(\mathbf{x})}{4\varepsilon^2}|u|^2 \,\mathrm{d}\mathbf{x}}{\int_{\mathbb{R}^N} |u|^2 \,\mathrm{d}\mathbf{x}}. \tag{3.2}$$

Defining the measure $\mathrm{d}\mathbf{p} = p(\mathbf{x})\,\mathrm{d}\mathbf{x}$, Rayleigh's quotient rewrites

$$\lambda_1 = \inf_{u \in D(L^\varepsilon)} \frac{\int_{\mathbb{R}^N} \varepsilon^2|\nabla u|^2 \,\mathrm{d}\mathbf{x} + \frac{1}{4\varepsilon^2}\int_{\mathbb{R}^N} |u|^2 \,\mathrm{d}\mathbf{p}}{\int_{\mathbb{R}^N} |u|^2 \,\mathrm{d}\mathbf{x}}.$$

LEMMA 2. *Let $\mathbf{x}_0$ be any point located at any positive and fixed distance from $\mathbf{0}$. Let $d > 0$: the first eigenvalue $\tilde{\lambda}_0$ associated with the operator,*

$$L^\varepsilon = -\varepsilon^2\Delta + \frac{p(\mathbf{x})}{4\varepsilon^2}, \qquad p(\mathbf{x}) = |\mathbf{x}|^2\chi_{B_R(\mathbf{0})} + d|\mathbf{x} - \mathbf{x}_0|^2\chi_{B_R(\mathbf{x}_0)}, \tag{3.3}$$

satisfies, for a positive constant value c, the following expansion:

$$\left|\tilde{\lambda}_0 - \frac{N}{2}\right| = O\left(\frac{R^2}{\varepsilon^2}\right)\exp\left(-\frac{cR^2}{\varepsilon^2}\right). \tag{3.4}$$

The shift between eigenvalues (3.4) and (2.11) comes from the factor $\frac{N}{2}$ in (2.1).

Proof. The Rayleigh quotient reads:

$$\tilde{\lambda}_0 = \min_{\psi\in H^1(\mathbb{R}^2)} \frac{\displaystyle\int_{\mathbb{R}^2} \varepsilon^2|\nabla\psi(\mathbf{x})|^2 + \frac{|\psi(\mathbf{x})|^2}{4\varepsilon^2}\left(|\mathbf{x}|^2\chi_{B_R(\mathbf{0})} + d|\mathbf{x}-\mathbf{x}_0|^2\chi_{B_R(\mathbf{x}_0)}\right)\,d\mathbf{x}}{\displaystyle\int_{\mathbb{R}^2}|\psi(\mathbf{x})|^2\,d\mathbf{x}}. \quad (3.5)$$

From Section 2, $\phi_0(\mathbf{x}) = \exp(-\frac{|\mathbf{x}|^2}{4\varepsilon^2})$ solves $-\varepsilon^2\Delta\phi_0 + \frac{|\mathbf{x}|^2}{4\varepsilon^2}\phi_0 = \frac{N}{2}\phi_0$, where

$$\begin{aligned}\frac{N}{2} = \lambda_0 &= \min_{\psi\ \in H^1(\mathbb{R}^2)} \frac{\displaystyle\int_{\mathbb{R}^2} \varepsilon^2|\nabla\psi(\mathbf{x})|^2 + \frac{|\mathbf{x}|^2}{4\varepsilon^2}|\psi(\mathbf{x})|^2\,d\mathbf{x}}{\displaystyle\int_{\mathbb{R}^2}|\psi(\mathbf{x})|^2\,d\mathbf{x}} \\ &= \frac{\displaystyle\int_{\mathbb{R}^2} \varepsilon^2|\nabla\phi_0(\mathbf{x})|^2 + \frac{|\mathbf{x}|^2}{4\varepsilon^2}|\phi_0(\mathbf{x})|^2\,d\mathbf{x}}{\displaystyle\int_{\mathbb{R}^2}|\phi_0(\mathbf{x})|^2\,d\mathbf{x}}.\end{aligned} \quad (3.6)$$

The explicit expression of λ_0, provided by the Rayleigh quotient, can be used in $\tilde{\lambda}_0$ in (3.5), in order to get the desired approximation. More precisely, by substituting $\phi_0(\mathbf{x})$ in the previous expression, the upper bound is given by

$$\begin{aligned}\tilde{\lambda}_0 \le \frac{N}{2} + \frac{1}{2\pi\varepsilon^2}\Bigg(&\int_{\mathbb{R}^2} \frac{|\mathbf{x}|^2\exp(-\frac{|\mathbf{x}|^2}{2\varepsilon^2})}{4\varepsilon^2}(\chi_{B_R(\mathbf{0})} - \mathbf{1})\,d\mathbf{x} \\ &+ \int_{\mathbb{R}^2} d|\mathbf{x}-\mathbf{x}_0|^2\chi_{B_R(\mathbf{x}_0)}\frac{\exp(-\frac{|\mathbf{x}|^2}{2\varepsilon^2})}{4\varepsilon^2}\,d\mathbf{x}\Bigg).\end{aligned}$$

On the other hand, the lower bound,

$$\begin{aligned}\tilde{\lambda}_0 &= \min_{\psi\ \in H^1(\mathbb{R}^2)} \frac{\displaystyle\int_{\mathbb{R}^2} \varepsilon^2|\nabla\psi(\mathbf{x})|^2 + \frac{|\psi(\mathbf{x})|^2}{4\varepsilon^2}\left(|\mathbf{x}|^2\chi_{B_R(\mathbf{0})} + d|\mathbf{x}-\mathbf{x}_0|^2\chi_{B_R(\mathbf{x}_0)}\right)\,d\mathbf{x}}{\displaystyle\int_{\mathbb{R}^2}|\psi(\mathbf{x})|^2\,d\mathbf{x}} \\ &= \min_{\psi\ \in H^1(\mathbb{R}^2)}\Bigg(\frac{\displaystyle\int_{\mathbb{R}^2} \varepsilon^2|\nabla\psi(\mathbf{x})|^2 + \frac{|\mathbf{x}|^2}{4\varepsilon^2}|\psi(\mathbf{x})|^2\,d\mathbf{x}}{\displaystyle\int_{\mathbb{R}^2}|\psi(\mathbf{x})|^2\,d\mathbf{x}} + \frac{\displaystyle\int_{\mathbb{R}^2}|\psi(\mathbf{x})|^2\frac{|\mathbf{x}|^2}{4\varepsilon^2}(\chi_{B_R(\mathbf{0})} - \mathbf{1})\,d\mathbf{x}}{\displaystyle\int_{\mathbb{R}^2}|\psi(\mathbf{x})|^2\,d\mathbf{x}} \\ &\qquad + \frac{\displaystyle\int_{\mathbb{R}^2}|\psi(\mathbf{x})|^2\frac{d|\mathbf{x}-\mathbf{x}_0|^2}{4\varepsilon^2}\chi_{B_R(\mathbf{x}_0)}\,d\mathbf{x}}{\displaystyle\int_{\mathbb{R}^2}|\psi(\mathbf{x})|^2\,d\mathbf{x}}\Bigg)\end{aligned}$$

$$\geq \min_{\psi\ \in H^1(\mathbb{R}^2)} \frac{\displaystyle\int_{\mathbb{R}^2} \varepsilon^2|\nabla\psi(\mathbf{x})|^2 + \frac{|\mathbf{x}|^2}{4\varepsilon^2}|\psi(\mathbf{x})|^2\,d\mathbf{x}}{\displaystyle\int_{\mathbb{R}^2}|\psi(\mathbf{x})|^2\,d\mathbf{x}} - \left(\frac{\displaystyle\int_{\mathbb{R}^2}|\tilde{\psi}(\mathbf{x})|^2\frac{|\mathbf{x}|^2}{4\varepsilon^2}(\chi_{B_R(\mathbf{0})}-\mathbf{1})\,d\mathbf{x}}{\displaystyle\int_{\mathbb{R}^2}|\tilde{\psi}(\mathbf{x})|^2\,d\mathbf{x}}\right.$$
$$\left. + \frac{\displaystyle\int_{\mathbb{R}^2}|\tilde{\psi}(\mathbf{x})|^2\frac{d|\mathbf{x}-\mathbf{x}_0|^2}{4\varepsilon^2}\chi_{B_R(\mathbf{x}_0)}\,d\mathbf{x}}{\displaystyle\int_{\mathbb{R}^2}|\tilde{\psi}(\mathbf{x})|^2\,d\mathbf{x}}\right),$$

where the last inequality holds for $\tilde{\psi}(\mathbf{x}) \in H^1(\mathbb{R}^2)$, being all the addends in the previous line positive. By using again (3.6) and setting $\tilde{\psi}(\mathbf{x}) = \phi_0(\mathbf{x})$, one gets

$$\tilde{\lambda}_0 \geq \frac{N}{2} - \frac{1}{2\pi\varepsilon^2}\left(\int_{\mathbb{R}^2}\frac{|\mathbf{x}|^2\exp(-\frac{|\mathbf{x}|^2}{2\varepsilon^2})}{4\varepsilon^2}(\chi_{B_R(\mathbf{0})}-\mathbf{1})\,d\mathbf{x}\right.$$
$$\left. + \int_{\mathbb{R}^2} d|\mathbf{x}-\mathbf{x}_0|^2\chi_{B_R(\mathbf{x}_0)}\frac{\exp(-\frac{|\mathbf{x}|^2}{2\varepsilon^2})}{4\varepsilon^2}\,d\mathbf{x}\right).$$

Passing to polar coordinates,

$$\frac{1}{2\pi\varepsilon^2}\int_{\mathbb{R}^2}\frac{|\mathbf{x}|^2}{4\varepsilon^2}(Id-\chi_{B_R(\mathbf{0})})|\phi_0(\mathbf{x})|^2\,\mathrm{d}\mathbf{x}$$
$$= \frac{1}{8\pi\varepsilon^4}\int_0^{2\pi}d\theta\int_R^{\infty}\rho^3\,\exp(-\frac{\rho^2}{2\varepsilon^2})\,\mathrm{d}\rho = \frac{(R^2+2\varepsilon^2)}{4\varepsilon^2}\exp(-\frac{R^2}{2\varepsilon^2}),$$
$$\int_{\mathbb{R}^2}\exp(-\frac{|\mathbf{x}|^2}{2\varepsilon^2})\,\mathrm{d}\mathbf{x} = 2\pi\varepsilon^2.$$

□

REMARK 1. *Lemma 2 implies that $\lambda_0 = \frac{N}{2}$ is a good approximation for the expression of the first eigenvalue when the potential only has two wells. Performing exactly the same computations with $\phi_0^d(\mathbf{x}) = \exp(-\frac{d|\mathbf{x}-\mathbf{x}_0|^2}{4\varepsilon^2})$, one gets $\lambda_0^d = \frac{Nd}{2}$. However, in this case the error term in the expansion is bigger, meaning that this approximation is less accurate than the one provided by the widest Gaussian.*

The parameter $d > 0$ in (3.3) controls the convexity of the well centered in $\mathbf{x}_0$. If the potential $p(\mathbf{x})$ has different wells, the ground state is known to accumulate only in one well, see [48, 27, 30]. From Lemma 2 (and Remark 1), the expression of the first eigenvalue $\tilde{\lambda}_0 = \frac{N}{2} + O\left(\frac{R^2}{\varepsilon^2}\right)\exp\left(-\frac{cR^2}{\varepsilon^2}\right)$ is reached by $\phi_0(\mathbf{x})$. This suggests that the accumulation well should be the one provided by $\frac{|\mathbf{x}|^2}{4\varepsilon^2}$.

DEFINITION 1 (see [42, 43]). *For a fixed $\tilde{\lambda} \in \mathbb{R}$, a quasi-eigenfunction is any function $u(\mathbf{x}) \in D(L^\varepsilon)$ such that the following "error function",*

$$\mathrm{Err}(u) := -\varepsilon^2\Delta u + \frac{p(\mathbf{x})}{4\varepsilon^2}u - \tilde{\lambda}u,$$

satisfies, for any $C(\varepsilon)$ exponentially decreasing, the inequality:

$$\|\mathrm{Err}(u)\|_{L^1(\mathbb{R}^N)} \leq C(\varepsilon), \qquad \varepsilon \ll 1.$$

In the next Lemma, we show that $\phi_0(\mathbf{x})$ is a quasi-eigenfunction of L^ε in (3.3), in the sense of Definition 1. Identical computations bring that

$$\phi_0^d(\mathbf{x}) := \exp\left(-\frac{d|\mathbf{x}-\mathbf{x}_0|^2}{4\varepsilon^2}\right)$$

is a quasi-eigenfunction of the operator defined in (3.3), too. However, it turns out that $\phi_0(\mathbf{x})$ is a better approximation of the ground-state of (3.3) than $\phi_0^d(\mathbf{x})$. The meaning of the last sentence is clarified below.

LEMMA 3. *Under the hypotheses of Lemma 2, let us fix $d > 1$. Then*

$$\|\mathrm{Err}(\phi_0)\|_{L^1(\mathbb{R}^N)} < \|\mathrm{Err}(\phi_0^d)\|_{L^1(\mathbb{R}^N)}, \qquad \phi_0^d(\mathbf{x}) = \exp(-\frac{d|\mathbf{x}-\mathbf{x}_0|^2}{4\varepsilon^2}). \tag{3.7}$$

Proof. Thanks to Lemma 2, in terms of the Rayleigh quotient,

$$\tilde{\lambda}_0 = \frac{N}{2} + O\left(\frac{R^2}{\varepsilon^2}\right)\exp\left(-\frac{cR^2}{\varepsilon^2}\right),$$

is reached by $\phi_0(\mathbf{x})$. This way, by comparing the two problems,

$$-\varepsilon^2\Delta\phi_0 + \frac{p(\mathbf{x})}{4\varepsilon^2}\phi_0 = \frac{N}{2}\phi_0 + \mathrm{Err}(\phi_0), \qquad -\varepsilon^2\Delta\phi_0^d + \frac{p(\mathbf{x})}{4\varepsilon^2}\phi_0^d = \frac{N}{2}\phi_0^d + \mathrm{Err}(\phi_0^d),$$

with $p(\mathbf{x})$ in (3.3), where

$$\mathrm{Err}(\phi_0) = \left[\frac{|\mathbf{x}|^2}{4\varepsilon^2}(\chi_{B_R(\mathbf{0})} - Id) + \frac{d|\mathbf{x}-\mathbf{x}_0|^2}{4\varepsilon^2}\chi_{B_R(\mathbf{x}_0)}\right]\phi_0,$$
$$\mathrm{Err}(\phi_0^d) = \left[\frac{d|\mathbf{x}-\mathbf{x}_0|^2}{4\varepsilon^2}(\chi_{B_R(\mathbf{x}_0)} - Id) + \frac{|\mathbf{x}|^2}{4\varepsilon^2}\chi_{B_R(\mathbf{0})} + \frac{N(d-1)}{2}\right]\phi_0^d,$$

and integrating in space, one gets (3.7). □ After proving that

- the best approximation for the first eigenvalue associated with L^ε in (3.3), $\tilde{\lambda}_0 \approx \frac{N}{2}$, is provided by $\phi_0(\mathbf{x})$ (Lemma 2),
- $\phi_0(\mathbf{x})$ is the best quasi-eigenfunction (Lemma 3),

we finally show that the solution to the spectral problem accumulates in $\frac{|\mathbf{x}|^2}{4\varepsilon^2}$, the widest well.

PROPOSITION 2. *Le $p(\mathbf{x})$ be a double well potential satisfying conditions [P]. Let $\mathbf{x}_1, \mathbf{x}_2$ be the centers of the two potential wells, and $\mathbf{x}_1$ be the widest one. The (normalized) solution $u(\mathbf{x}) \in H^1(K^\varepsilon)$ to the spectral problem associated with (3.3) accumulates in the widest well. More precisely, for a fixed $\varepsilon > 0$, let $B_R(\mathbf{x}_i)$ be the disk of radius $R > 0$ and center $\mathbf{x}_i$, $i = 1, 2$, there exists $\varepsilon_0 > 0$ such that,*

$$\boxed{\forall \varepsilon \le \varepsilon_0, \qquad \int_{B_R(\mathbf{x}_1)} |u(\mathbf{x})|^2\, d\boldsymbol{p} > \exp\left(\frac{c|\mathbf{x}_1-\mathbf{x}_2|^2}{\varepsilon^2}\right)\int_{B_R(\mathbf{x}_2)} |u(\mathbf{x})|^2\, d\boldsymbol{p}.}$$

Proof. Without loss of generality, we consider L^ε in (3.3). The first eigenfunction is well approximated by $\phi_0(\mathbf{x})$. This way,

$$\int_{B_R(\mathbf{0})} |\phi_0(\mathbf{x})|^2\, d\mathbf{p} = \int_{B_R(\mathbf{0})} |\phi_0(\mathbf{x})|^2 \frac{|\mathbf{x}|^2}{4\varepsilon^2}\, d\mathbf{x} = 2\pi \int_0^R \exp(-\frac{\rho^2}{2\varepsilon^2})\, \rho^3\, d\rho;$$

$$\begin{aligned}\int_{B_R(\mathbf{x}_0)} |\phi_0(\mathbf{x})|^2\, d\mathbf{p} &= \int_{B_R(\mathbf{x}_0)} |\phi_0(\mathbf{x})|^2 \frac{d|\mathbf{x}-\mathbf{x}_0|^2}{2\varepsilon^2}\, d\mathbf{x} \\ &= d\exp(-\frac{|\mathbf{x}_0|^2}{2\varepsilon^2}) \int_0^{2\pi} d\theta \int_0^R \exp(\frac{-\rho^2 - 2\rho x_0\cos\theta - 2\rho y_0 \sin\theta}{2\varepsilon^2})\, \rho^3\, d\rho \\ &\geq 2\pi d \exp(-\frac{|\mathbf{x}_0|^2}{\varepsilon^2}) \int_0^R \exp(-\frac{\rho^2}{\varepsilon^2})\, \rho^3\, d\rho,\end{aligned}$$

which ends the proof. □

3.2. Distance from the wells. Given a potential well and a localized perturbation: does the distance between each other affect the spectral problem ? If wells are far enough from each other, this is a local question which is addressed by perturbing the harmonic potential. Hereafter, $\varepsilon = 1$ and the term $\frac{N}{2}$ in (2.1) is ignored,

$$L(u) = -\Delta u + \frac{|\mathbf{x}|^2}{4} u, \qquad \phi_0(\mathbf{x}) = \exp(-\frac{|\mathbf{x}|^2}{4}). \tag{3.8}$$

Let a small perturbation be given by $\chi_{B_R(\mathbf{x}_0)}(\mathbf{x})$, the characteristic function of a disk centered in $\mathbf{x}_0$ of radius $R > 0$, and consider a perturbed spectral problem,

$$L^R(u) = -\Delta u + \frac{|\mathbf{x}|^2}{4} u + \chi_{B_R(\mathbf{x}_0)} u = \lambda u. \tag{3.9}$$

The ground-state $\phi_0(x)$ of (3.8) can be seen as an *quasi-eigenfunction* for the perturbed problem (3.9), as it almost satisfies the spectral equation for $L^R(u)$,

$$-\Delta\phi_0 + \frac{|x|^2}{4}\phi_0 + \chi_{B_R(\mathbf{x}_0)}\phi_0 \approx \lambda\phi_0,$$

with an error

$$\mathrm{Err}(\mathbf{x}_0) = \chi_{B_R(\mathbf{x}_0)}\phi_0(\mathbf{x}) = \chi_{B_R(\mathbf{x}_0)} \exp(-\frac{|\mathbf{x}|^2}{4}).$$

In one dimension, $N = 1$, such an error is easy to quantify, for instance in L^1,

$$x_0 \mapsto \|\mathrm{Err}(x_0)\|_{L^1(\mathbb{R})} = \int_{x_0-R}^{x_0+R} \exp(-\frac{|x|^2}{4})\, \mathrm{d}x.$$

so that its variations with respect to $x_0 \in \mathbb{R}$ satisfy:

$$\frac{d}{dx_0}\|\mathrm{Err}(x_0)\|_{L^1(\mathbb{R})} = \exp(-\left|\frac{x_0+R}{2}\right|^2) - \exp(-\left|\frac{x_0-R}{2}\right|^2) = \begin{cases} < 0, & (x_0 > 0), \\ > 0, & (x_0 < 0). \end{cases}$$

This derivative shows that,

- the position $x_0 = 0$ is a local maximum for $\|\mathrm{Err}(x_0)\|_{L^1(\mathbb{R})}$;
- the perturbation's effects on (3.8) decrease with both $|x_0|$ and R.

This elementary argument can be extended to N dimensions; precise results on the role of the position of the perturbation are given in, *e.g.* [48].

3.3. Variations of the spectral components. Coming back to a general potential $p(\mathbf{x})$ in (3.1), we consider $L(u)$ in (3.8), where λ, u are any eigenvalue and normalized eigenfunction. Let M be any linear bounded operator and $\delta \ll 1$ a constant small enough: again, we treat λ as a *quasi-eigenvalue* for the perturbed operator,

$$Lu + \delta Mu = \lambda u + Err^{\delta}(u), \qquad \text{where} \qquad Err^{\delta}(u) = \delta Mu. \tag{3.10}$$

We take the derivative of (3.10) w.r.t. δ, calculated in $\delta = 0$,

$$Lu' + Mu = \lambda' u + \lambda u' + O(\|Mu\|), \qquad \text{where } \cdot' := \left.\frac{d}{d\delta}\right|_{\delta=0}$$

Namely,

$$(L - \lambda)u' = (\lambda' - M)u + O(\|Mu\|). \tag{3.11}$$

Since λ is an eigenvalue of L, associated with the eigenfunction u, then $u \in Ker(L-\lambda)$. Fredholm's Alternative implies that there exist solutions u' to (3.11) such that

$$(\lambda' - M)u + O(\|Mu\|) \perp Ker(L - \lambda),$$

i.e., denoting by $< \cdot, \cdot >$ the L^2 scalar product,

$$< (\lambda' - M)u, u >= O(\|Mu\|), \qquad \|u\|^2 =< u, u >= 1,$$

then,

$$\lambda' = \left.\frac{d}{d\delta}\right|_{\delta=0} \lambda(\delta) =< Mu, u > +O(\|Mu\|), \tag{3.12}$$

namely

$$|\lambda'| \leq \|Mu\|\|u\| + O(\|Mu\|) = \|Mu\| + O(\|Mu\|),$$

so that the perturbation δM affects eigenvalues according to the way M affects the original eigenfunction u. Yet, we look at the variations of this eigenfunction by taking the derivative with respect to δ of the scalar product $\|u\|^2 =< u, u >= 1$.

$$\frac{1}{2}\left.\frac{d}{d\delta}\right|_{\delta=0} (\|u\|^2) =< u, u' >= 0, \quad \text{i.e.} \quad u' \perp u.$$

Orthogonality $u' \perp u$ and $(L - \lambda)u' \perp u$, along with Fredholm's Alternative imply

$$u' \quad \text{is proportional to} \quad (\lambda' - M)u + O(\|Mu\|) = (L - \lambda)u',$$

so that, locally for $\delta \simeq 0$,

$$\|u'\| \leq C\|Mu\| \quad \text{for a given constant value} \quad C(\lambda).$$

4. Two-dimensional "Steklov numerical scheme". In this section, a derivation is recalled from [17], in order to establish several properties in close relation with the original problem of the "flea on the elephant". Hereafter, we shall always work on a uniform, Cartesian computational grid, with $\Delta x = \Delta y$.

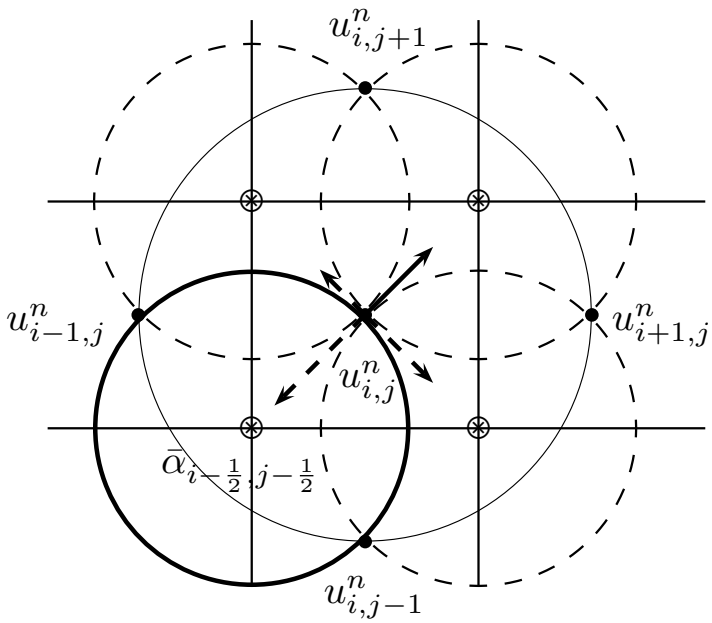

FIGURE 4.1. *Transmission conditions at $u^n_{i,j}$ given by Steklov-Poincaré operators.*

4.1. Derivation of the numerical process. Consider the stationary, strictly elliptic and coercive, two-dimensional problem,

$$\begin{cases} -\Delta u + \alpha^2(x,y)u = 0, & (x,y) \in \Omega, \\ u(x,y) = g(x), & (x,y) \in \partial\Omega, \end{cases} \tag{4.1}$$

where Ω is a polygonal domain of $\mathbb{R}^2$. The numerical simulations, carried out with the "Steklov scheme" [17], and presented below mostly focus on the spectral analysis associated with the strictly elliptic operator $L(u) := -\Delta u + \alpha^2(x,y)u$. Accordingly, we shall work on the square (Lipschtiz) domain $\Omega = (0,1)^2 \subset \mathbb{R}^2$, so that the typical regularity for u should be at least $H^2(\Omega)$, see [8, 21]. We refer to Appendix A for elementary regularity results for problems like (4.1) in a square domain: in particular, when the *compatibility conditions* (A.2) hold at each corner, the Hölder regularity of inhomogeneous Dirichlet data g passes to the solution u, see Theorem A.2.

The "Steklov scheme", see [17, 18] works in the following way: (see Fig. 4.1)

- at each "node", $(x_{i-\frac{1}{2}}, y_{j-\frac{1}{2}})$, the potential is "frozen", so that

$$\bar{\alpha}^2_{i-\frac{1}{2},j-\frac{1}{2}} := \alpha^2(x_{i-\frac{1}{2}}, y_{j-\frac{1}{2}}), \qquad i,j \in \mathbb{Z}^2;$$

- in each disk $D_R(i-\frac{1}{2}, j-\frac{1}{2})$, centered at a node,

$$D_R(i-\frac{1}{2}, j-\frac{1}{2}) = \Big\{ |x - x_{i-1/2}|^2 + |y - y_{j-1/2}|^2 \le R^2 \Big\}, \qquad R = \frac{\Delta x}{\sqrt{2}},$$

the following problem is explicitly solved in polar coordinates,

$$\begin{cases} -\Delta v + \bar{\alpha}^2_{i-\frac{1}{2},j-\frac{1}{2}} v = 0, & (x,y) \in D_R, \\ v = g \text{ on the boundary}, & (x,y) \in C_R := \partial D_R, \end{cases} \tag{4.2}$$

by means of Fourier-Bessel series involving "modified Bessel functions", $\mathcal{I}_n(\cdot)$. Note that, as shown in Figure 4.1, in the discrete framework we only consider exactly three values of the trace of v at the boundary $C_R(i-\frac{1}{2}, j-\frac{1}{2})$, i.e., $v(x_i, y_j), v(x_{i-1}, y_j), v(x_i, y_{j-1})$. However, at the moment let us consider the BVP (4.2) at the formal level, keeping in mind that precise trace estimates on the discrete approximation of g in (4.2) will be discussed in Section 4.2.

- The exact solution of the stationary BVP (4.2) reads,

$$v(r,\theta) = A_0\mathcal{I}_0(\bar{\alpha}r) + \sum_{n\in\mathbb{N}}(A_n\cos n\theta + B_n \sin n\theta)\mathcal{I}_n(\bar{\alpha}r), \qquad r \le R, \quad (4.3)$$

where $\bar{\alpha} = \bar{\alpha}_{i-\frac{1}{2},j-\frac{1}{2}}$, and coefficients are determined by the boundary data prescribed on the circle $C_R(i-\frac{1}{2}, j-\frac{1}{2})$. More precisely, if we are given a boundary condition $g \in H^s(0, T = 2\pi R)$, then it admits a Fourier series,

$$g(x) = a_0 + \sum_{n\in\mathbb{N}} a_n \cos(\frac{2\pi n\, x}{T}) + b_n \sin(\frac{2\pi n\, x}{T}),$$

so that, setting $r = R$ in (4.3), and by uniqueness, we have

$$A_0 = \frac{a_0}{\mathcal{I}_0(\bar{\alpha}R)}, \qquad A_n = \frac{a_n}{\mathcal{I}_n(\bar{\alpha}R)}, \qquad B_n = \frac{b_n}{\mathcal{I}_n(\bar{\alpha}R)}, \quad (4.4)$$

meaning that the solution to (4.2) is completely known.

- At this point, the main idea to derive the Steklov scheme, see [17, 18], is based on the discretization of the normal derivative of the solution $v(r,\theta)$ in (4.3), obtained by means of the Steklov-Poincaré operator. Since the domain is circular, the normal derivative reduces to the radial one, and the Steklov-Poincaré operator can be made explicit,

$$\frac{1}{\bar{\alpha}}\frac{\partial v}{\partial r}(R,\theta) = A_0\mathcal{I}_1(\bar{\alpha}R) + \sum_{n\in\mathbb{N}}(A_n\cos n\theta + B_n\sin n\theta)\frac{\mathcal{I}_{n-1}+\mathcal{I}_{n+1}}{2}(\bar{\alpha}R),$$

and, by using identities (4.4), this rewrites,

$$\frac{1}{\bar{\alpha}}\frac{\partial v}{\partial r}(R,\theta) = a_0\frac{\mathcal{I}_1}{\mathcal{I}_0}(\bar{\alpha}R) + \sum_{n\in\mathbb{N}}(a_n\cos n\theta + b_n\sin n\theta)\frac{\mathcal{I}_{n-1}+\mathcal{I}_{n+1}}{2\mathcal{I}_n}(\bar{\alpha}R). \quad (4.5)$$

- In practice, as anticipated before, we never have all the Fourier coefficients at hand, because there are at most four discrete (grid) numerical values,

$$P_k = R(\cos\theta_k, \sin\theta_k), \quad 0 \le k \le 2, \qquad \theta_k = \frac{k\pi}{2}, \quad (4.6)$$

on each circle $C_R(i\pm\frac{1}{2}, j\pm\frac{1}{2})$, so the former series are truncated at $n \le 1$,

$$\frac{1}{\bar{\alpha}}\frac{\partial v}{\partial r}(R,\theta) = a_0\frac{\mathcal{I}_1}{\mathcal{I}_0}(\bar{\alpha}R) + (a_1\cos\theta + b_1\sin\theta)\frac{\mathcal{I}_0+\mathcal{I}_2}{2\mathcal{I}_1}(\bar{\alpha}R). \quad (4.7)$$

The explicit expressions of coefficients a_0, a_1, b_1 are obtained by means of (4.3), truncated at $n \le 1$, to each grid value P_k in (4.6) of the circle's boundary $C_R(i-\frac{1}{2}, j-\frac{1}{2})$. Precisely, expression (4.3) with identities (4.4) gives

$$\begin{cases} P_0 = v(R,\theta=0) = u^n_{i,j} = A_0\mathcal{I}_0(\bar{\alpha}R) + A_1\mathcal{I}_1(\bar{\alpha}R), \\ P_1 = v(R,\theta=\frac{\pi}{2}) = u^n_{i-1,j} = A_0\mathcal{I}_0(\bar{\alpha}R) + B_1\mathcal{I}_1(\bar{\alpha}R), \\ P_2 = v(R,\theta=-\frac{\pi}{2}) = u^n_{i,j-1} = A_0\mathcal{I}_0(\bar{\alpha}R) - B_1\mathcal{I}_1(\bar{\alpha}R), \end{cases}$$

yield:

$$\begin{cases} a_0 = A_0\mathcal{I}_0(\bar{\alpha}R) = \dfrac{u^n_{i-1,j} + u^n_{i,j-1}}{2}, \\ a_1 = A_1\mathcal{I}_1(\bar{\alpha}R) = u^n_{i,j} - \dfrac{u^n_{i-1,j} + u_{i,j-1}}{2}, \\ b_1 = B_1\mathcal{I}_1(\bar{\alpha}R) = \dfrac{u^n_{i-1,j} - u^n_{i,j-1}}{2}. \end{cases} \tag{4.8}$$

Inserting (4.8) into (4.7),

$$\frac{1}{\bar{\alpha}}\frac{\partial v}{\partial r}(R,\theta) = \left\{ u^n_{i,j}\frac{\mathcal{I}_0+\mathcal{I}_2}{2\mathcal{I}_1}\cos\theta + u^n_{i-1,j}\left[\frac{\mathcal{I}_1}{2\mathcal{I}_0} + \frac{\mathcal{I}_0+\mathcal{I}_2}{4\mathcal{I}_1}(\sin\theta - \cos\theta)\right] + u^n_{i,j-1}\left[\frac{\mathcal{I}_1}{2\mathcal{I}_0} - \frac{\mathcal{I}_0+\mathcal{I}_2}{4\mathcal{I}_1}(\sin\theta + \cos\theta)\right]\right\}(\bar{\alpha}R). \tag{4.9}$$

In the end, by using the regularity of the solution to the considered BVP, the Steklov scheme is derived by balancing the four normal (radial) derivatives for each circle $C_R(i \pm \frac{1}{2}, j \pm \frac{1}{2})$,

$$\begin{aligned} &\frac{\partial v}{\partial r}(R,0)(\bar{\alpha}_{i-\frac{1}{2},j-\frac{1}{2}}R) + \frac{\partial v}{\partial r}(R,\frac{\pi}{2})(\bar{\alpha}_{i-\frac{1}{2},j+\frac{1}{2}}R) \\ &+ \frac{\partial v}{\partial r}(R,\pi)(\bar{\alpha}_{i+\frac{1}{2},j+\frac{1}{2}}R) + \frac{\partial v}{\partial r}(R,\frac{3\pi}{2})(\bar{\alpha}_{i+\frac{1}{2},j-\frac{1}{2}}R) = 0, \end{aligned} \tag{4.10}$$

and so the following numerical scheme is obtained,

$$\begin{aligned} u_{i,j}&\Big\{\mathcal{F}(\bar{\alpha}_{i-\frac{1}{2},j-\frac{1}{2}}) + \mathcal{F}(\bar{\alpha}_{i+\frac{1}{2},j-\frac{1}{2}}) + \mathcal{F}(\bar{\alpha}_{i+\frac{1}{2},j+\frac{1}{2}}) + \mathcal{F}(\bar{\alpha}_{i-\frac{1}{2},j+\frac{1}{2}})\Big\} \\ &+ u_{i-1,j}\Big\{\mathcal{G}(\bar{\alpha}_{i-\frac{1}{2},j-\frac{1}{2}}) + \mathcal{G}(\bar{\alpha}_{i-\frac{1}{2},j+\frac{1}{2}})\Big\} \\ &+ u_{i,j-1}\Big\{\mathcal{G}(\bar{\alpha}_{i-\frac{1}{2},j-\frac{1}{2}}) + \mathcal{G}(\bar{\alpha}_{i+\frac{1}{2},j-\frac{1}{2}})\Big\} \\ &+ u_{i+1,j}\Big\{\mathcal{G}(\bar{\alpha}_{i+\frac{1}{2},j-\frac{1}{2}}) + \mathcal{G}(\bar{\alpha}_{i+\frac{1}{2},j+\frac{1}{2}})\Big\} \\ &+ u_{i,j+1}\Big\{\mathcal{G}(\bar{\alpha}_{i+\frac{1}{2},j+\frac{1}{2}}) + \mathcal{G}(\bar{\alpha}_{i-\frac{1}{2},j+\frac{1}{2}})\Big\} = 0, \end{aligned} \tag{4.11}$$

where

$$\boxed{\mathcal{F}(\alpha) = \alpha\frac{\mathcal{I}_0+\mathcal{I}_2}{2\mathcal{I}_1}(\alpha R), \quad \mathcal{G}(\alpha) = \frac{\mathcal{H}(\alpha)-\mathcal{F}(\alpha)}{2}, \quad \mathcal{H}(\alpha) = \alpha\frac{\mathcal{I}_1}{\mathcal{I}_0}(\alpha R).}$$

Standard results for $\mathcal{I}_n(\cdot)$ imply that both $\mathcal{F}(\alpha)$ and $\mathcal{G}(\alpha)$ behave like $O(1/R)$ when $\bar{\alpha}R \ll 1$ and $O(1)$ when $\bar{\alpha}R \gg 1$. Moreover, (4.11) was proved to be consistent with (4.1) and monotone (hence, positivity-preserving) in [17].

Yet, consider a $N \times N$ two-dimensional grid (N^2 internal points), and given the $2D$ array of values $u_{i,j}$, define the following one-dimensional vector,

$$\mathbf{U}^N = \Big[u_{1,1}, u_{2,1}, \cdots, u_{N,1}, \quad u_{1,2}, \cdots, u_{N,2}, \quad \cdots\cdots\cdots, \quad u_{1,N}, \cdots, u_{N,N}\Big]. \tag{4.12}$$

Identity (4.11) recasts in matrix form like,

$$P^N\mathbf{U}^N = B, \qquad P^N \text{ a } (N^2 \times N^2) \text{ matrix}, \tag{4.13}$$

where B stands for discretized boundary data.

LEMMA 4. *Matrix P^N in (4.13) is a symmetric M-matrix.*

Proof. Let $C_{i,j}(\mathcal{S}_{i,j})$ be the general coefficient of the term $u_{i,j}$, where $\mathcal{S}_{i,j}$ indicates in which grid's point $\mathbf{x}_{i,j}$ relation (4.11) is used. It is straightforward to check that

- $C_{i+1,j}(\mathcal{S}_{i,j}) = C_{i,j}(\mathcal{S}_{i+1,j}) = \mathcal{G}(\bar{\alpha}_{i+1/2,j-1/2}) + \mathcal{G}(\bar{\alpha}_{i+1/2,j+1/2}), \quad i,j \geq 1;$
- $C_{i,j+1}(\mathcal{S}_{i,j}) = C_{i,j}(\mathcal{S}_{i,j+1}) = \mathcal{G}(\bar{\alpha}_{i+1/2,j+1/2}) + \mathcal{G}(\bar{\alpha}_{i-1/2,j+1/2}), \quad i,j \geq 1;$
- $C_{i-1,j}(\mathcal{S}_{i,j}) = C_{i,j}(\mathcal{S}_{i-1,j}) = \mathcal{G}(\bar{\alpha}_{i-1/2,j-1/2}) + \mathcal{G}(\bar{\alpha}_{i-1/2,j+1/2}), \ i \geq 2, j \geq 1;$
- $C_{i,j-1}(\mathcal{S}_{i,j}) = C_{i,j}(\mathcal{S}_{i,j-1}) = \mathcal{G}(\bar{\alpha}_{i+1/2,j-1/2}) + \mathcal{G}(\bar{\alpha}_{i-1/2,j-1/2}), \ i \geq 1, j \geq 2.$

A sufficient condition for P^N being a M-matrix is that:

- its principal diagonal is strictly positive,
- other entries are negative or null,
- it is diagonally-dominant.

All these properties follow from (4.11) because, for any n, $\mathcal{I}_n(x) \geq 0$ for $x \geq 0$ and they are monotonically increasing. □

Accordingly, P^N has a positive inverse, uniformly in $\|\alpha^2\|_\infty R$. A useful estimate is the minimum of its eigenvalues, because $\|(P^N)^{-1}\|_2 \leq 1/\min(\mu_\ell)$. Such a number can be explicitly computed (see [11, pages 179–181] and [52]) when the potential is a constant, $\alpha^2 \in \mathbb{R}^+$: being P^N block-diagonal (with $N \times N$ blocks),

$$\begin{cases} \mu_\ell = 4\,\mathcal{F}(\alpha) + 8\,\mathcal{G}(\alpha)\cos(\pi\Delta x), \\ \left\|(P^N)^{-1}\right\|_2 \leq \dfrac{1}{4(\mathcal{F}(\alpha) + 2\mathcal{G}(\alpha)\cos(\pi\Delta x))}. \end{cases} \tag{4.14}$$

Before studying the truncation errors of (4.11), we stress that such a monotone discretization of (4.1) is a good candidate for problems which develop sharp layers. Indeed, the modified Bessel functions $\mathcal{I}_n$ display an exponential behavior at infinity, so that (4.11) can be fairly considered a "two-dimensional exponential-fit scheme".

4.2. Truncated series and "localized sampling". As mentioned before, in practice, it is necessary to truncate the Fourier-Bessel series of the exact solution $v(r,\theta)$, because only 4 grid points are available on each circle $C_R(i \pm \frac{1}{2}, j \pm \frac{1}{2})$ (instead of boundary data of co-dimension 1), and for the present scheme, we use only 3. In this section, we provide an estimate of the approximation due to this 3-points discretization on each one of the four circles of the stencil, by comparison with the 4-points discretization, which results to be an application of the trapezoidal integration rule. Hereafter, consider $h(\theta) \in H^s(0, 2\pi)$, 2π-periodic, that is approximated by two different trigonometric polynomials,

$$\begin{cases} h_4(\theta) &= \mathbf{a}_0 + \mathbf{a}_1\cos\theta + \mathbf{b}_1\sin\theta + \mathbf{a}_2\cos 2\theta, \\ h_3(\theta) &= \alpha_0 + \alpha_1\cos\theta + \beta_1\sin\theta, \end{cases}$$

both of them being determined by imposing,

$$\begin{cases} h_4(0) = c, \qquad h_4(\frac{\pi}{2}) = a, \qquad h_4(\pi) = d, \qquad h_4(-\frac{\pi}{2}) = b, \\ \qquad\quad h_3(0) = c, \qquad h_3(\frac{\pi}{2}) = a, \qquad h_3(-\frac{\pi}{2}) = b. \end{cases}$$

Hence, given any 4 generic points on a circle C_R, coefficients read:

$$\mathbf{a}_0 = \frac{1}{4}(a+b+c+d), \qquad \mathbf{b}_1 = \frac{1}{2}(a-b),$$
$$\mathbf{a}_1 = \frac{1}{2}(c-d), \qquad \mathbf{a}_2 = \frac{c+d}{4} - \frac{a+b}{4},$$

so that,

$$\mathbf{a}_0 = O(1), \qquad \mathbf{a}_1, \mathbf{b}_1 = O(R), \qquad \mathbf{a}_2 = O(R^2),$$

along with

$$\alpha_0 = \frac{1}{2}(a+b), \qquad \alpha_1 = c - \frac{1}{2}(a+b), \qquad \beta_1 = \frac{1}{2}(a-b).$$

The polynomial h_3 is sometimes referred to as to a "localized sampling" because, oppositely to h_4, it interpolates only the 3 points which are the closest to the location where the radial derivative is meant to be computed. Despite their coefficients are distinct, their difference $h_4 - h_3$ depends only on $\mathbf{a}_2$: indeed,

$$\begin{aligned}(h_4 - h_3)(\theta) &= (\mathbf{a}_0 - \alpha_0) + (\mathbf{a}_1 - \alpha_1)\cos\theta + \mathbf{a}_2 \cos 2\theta \\ &= \mathbf{a}_2(1 - 2\cos\theta + \cos 2\theta).\end{aligned} \tag{4.15}$$

The fact that the gap $h_3 - h_4$ is like $\mathbf{a}_2$, a "trapezoidal approximation", is essential.

4.3. Local truncation error. If the circular trace of a 2D function $u(x, y)$, has a very small "mixed derivative", $|\partial^2_{xy} u| \ll 1$, then $\mathbf{a}_2 \simeq 0$. Accordingly, define

$$g(x) = h(R\theta), \qquad g : (0, T = 2\pi R) \to \mathbb{R}, \qquad g \text{ is } T\text{-periodic}.$$

It isn't easy to estimate the (curvilinear) derivatives of g with respect to the abscissa x because of the circle's curvature, which equals $\frac{1}{R}$:

$$\begin{aligned}\frac{\mathrm{d}g}{\mathrm{d}x} &= \frac{1}{R}\frac{\mathrm{d}g}{\mathrm{d}\theta} = -\partial_x u(R\cos\theta, R\sin\theta)\sin\theta + \partial_y u(R\cos\theta, R\sin\theta)\cos\theta, \\ \frac{\mathrm{d}^2 g}{\mathrm{d}x^2} &= -\frac{1}{R}\Big(\partial_x u(R\cos\theta, R\sin\theta)\cos\theta + \partial_y u(R\cos\theta, R\sin\theta)\sin\theta\Big) + ...,\end{aligned}$$

hence a "bad term" $\frac{1}{R}\frac{\partial u}{\partial r}$ appears in the second derivative of g. This complicates the control of errors produced when approximating h with both h_4 and h_3. To estimate the noise induced by the "localized sampling" of only 3 grid points,

$$\|g - g_3\|_{L^2(0,T)} \le \|g - g_4\|_{L^2(0,T)} + \|g_4 - g_3\|_{L^2(0,T)},$$

and we proceed thanks to the elementary observation:

$$\|g_4 - g_3\|^2_{L^2(0,T)} = |\mathbf{a}_2|^2 \int_0^T \left|1 - 2\cos(\frac{x}{R}) + \cos(\frac{2x}{R})\right|^2 \mathrm{d}x = T(1+4+1)|\mathbf{a}_2|^2.$$

Lemma 5. *Let $u \in H^s(\mathbb{R}^2)$, $s \ge N + \frac{1}{2}$, and $f : (0, T = 2\pi R) \to \mathbb{R}$ its trace on a circle of radius $R > 0$. Define the "N-points approximation" of its average $\hat{f}(0)$ as,*

$$\hat{f}_N(0) := \frac{1}{N}\sum_{j=0}^{N-1} f(j\frac{T}{N}), \quad \hat{f}(0) = \frac{1}{T}\int_0^T f(x)\mathrm{d}x = \frac{1}{2\pi}\int_0^{2\pi} f(\theta)\mathrm{d}\theta, \quad \theta = \frac{x}{R},$$

then, either

- *the method is exact, $\hat{f}(0) = \hat{f}_N(0)$ if $\hat{f}(k) \equiv 0$ when $|k| \ge N$;*
- *or its error satisfies $|\hat{f}(0) - \hat{f}_N(0)| \le \sum_{k\in\mathbb{Z}_*} |\hat{f}(Nk)| \le O(R^N)$.*

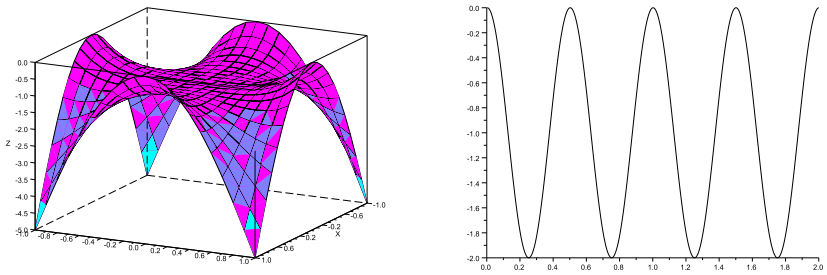

FIGURE 4.2. *Counter-example of [4, Thm. 7]: polynomial (left) and its trace on* $\mathcal{C}(0,\Delta x)$ *(right).*

Proof. See Appendix B. □

REMARK 2. *Theorem 7 in [4] states that the LTE of the classical 5-points scheme for Laplace's equation*[1]*, being the limit* $\bar{\alpha}\to 0$ *of (4.11, is of order* Δx^4*. Its proof draws on the harmonic polynomial, the real part of* $(x+iy)^4-\Delta x^4$*, see Fig. 4.2,*

$$p(x,y)=x^4-6x^2y^2+y^4-\Delta x^4,\qquad (x,y)\in(-\Delta x,\Delta x)^4,$$

for which $p(\pm\Delta x,\pm\Delta x)=0$*, but* $p(0,0)=\Delta x^4\neq 0$*. Its trace on the circle centered at the origin, of radius* Δx*,* $\mathcal{C}(0,\Delta x)$*, is displayed on Fig. 4.2 (right) and reads*

$$p(\Delta x\cos\theta,\Delta x\sin\theta)=\Delta x^4\big(\cos^4\theta-6\cos^2\theta\sin^2\theta+\sin^4\theta-1\big)=\Delta x^4\big(\cos(4\theta)-1\big).$$

Lemma 5 applies to that simple case because, for any harmonic function $u\in H^{\frac{9}{2}}(\mathbb{R}^2)$*,*

$$\begin{aligned}u(0,0)&=\frac{1}{2\pi R}\int_{\mathcal{C}(0,R)}u(x,y)\,\mathrm{d}\ell\\&=\frac{1}{4}\big(u(R,0)+u(0,R)+u(-R,0)+u(0,-R)\big)+O(R^4),\end{aligned}$$

and picking $R=\Delta x$*, one recovers both second-order accuracy for general solutions, and the exactness of the method if no frequencies higher than* $|k|=3$ *are present. Such bounds apply to "discrete weighted means" [15] and "tailored methods" [23], too.*

The discrepancy between boundary data which involves the exact Fourier coefficients $\hat{g}(k)$ and the one involving $\alpha_0,\alpha_1,\beta_1$ is: (since g is real, $\hat{g}(k)=\hat{g}(-k)^*$)

$$|\hat{g}(0)-\alpha_0|^2+|2\Re(\hat{g}(1))-\alpha_1|^2+\big|i\big(\hat{g}(1)-\hat{g}(-1)\big)-\beta_1\big|^2+\sum_{|k|>1}|\hat{g}(k)|^2.$$

THEOREM 4.1. *Consider the problem (4.1) with the coefficient* $\alpha\equiv\bar{\alpha}$ *being constant, and a corresponding solution* $u(x,y)$*:*

- *if* $u\in C^4$*, the global* L^2 *error of (4.11) is second-order as* $\Delta x\to 0$*;*
- *if* $\hat{g}(k)=0$ *for* $|k|\geq 2$*, the approximation (4.10) matches the exact one (4.5).*

Proof. We establish each statement independently for the sake of clarity:

[1] which is *exact* for linear solutions of $\Delta u=0$. In 2D, there are only two linearly independent homogeneous harmonic polynomials of degree m : the real and imaginary part of $(x+iy)^m$.

- Given a point x_i, y_j, the local truncation error (LTE) is the discrepancy $\tau_{i,j} := \tau(x_i, y_j)$ which remains when pointwise values of u, the exact solution to (4.1) are inserted into the scheme (4.11). By grouping terms, it comes,

$$\begin{aligned} 0 &= \mathcal{F}(\bar{\alpha})\Big(4u_{i,j} - u_{i\pm1,j\pm1}\Big) + \mathcal{H}(\bar{\alpha})u_{i\pm1,j\pm1} \\ &= \mathcal{F}(\bar{\alpha}R)\Big(- \Delta x^2\, \Delta u(x_i, y_j) + O(\Delta x^4)\Big) + 4\mathcal{H}(\bar{\alpha})\Big(u(x_i, y_j) + O(\Delta x^2)\Big), \end{aligned}$$

so that, by performing Taylor expansions of $\mathcal{I}_n(\bar{\alpha}R)$ with $0 \leq \bar{\alpha}R \ll 1$,

$$\mathcal{F}(\bar{\alpha}) = \frac{1}{R} + O(R), \qquad \mathcal{H}(\bar{\alpha}) = \bar{\alpha}^2\frac{R}{2} + O(R^3),$$

and the LTE is $O(R^3)$. To deduce the global error of the scheme, the L^2 norm is computed by means of pointwise values,

$$\|u - u_{\Delta x}\|_{L^2}^2 = \Delta x^2 \sum_{i,j} |u(x_i, y_j) - u_{i,j}|^2. \tag{4.16}$$

Thanks to the linearity of the scheme (4.11)–(4.13),

$$P^N(u) - P^N(u_{\Delta x}) = \tau = P^N(u - u_{\Delta x}),$$

being τ the formerly derived LTE. The global L^2 error is controlled by,

$$\|u - u_{\Delta x}\|_{L^2}^2 = \|(P^N)^{-1}\,\tau\|_{L^2}^2 \leq \left\|(P^N)^{-1}\right\|_2^2 \|\tau\|_{L^2}^2,$$

and the bound (4.14) on P^N. Second-order accuracy follows from,

$$\left\|(P^N)^{-1}\right\|_2 = O(\frac{1}{R}) \text{ when } 0 \leq \bar{\alpha}R \ll 1.$$

- We study the deviation between the exact derivatives (4.5) and the truncated ones (4.7), used in (4.10), which involve only the first 3 terms of the Fourier expansion (4.3). Since exact modified Bessel functions are used in the solution $v(r, \theta)$ to (4.2) along with its radial derivatives (4.9), we must control

$$\begin{aligned} &\left|\frac{\mathcal{I}_0 + \mathcal{I}_2}{2\mathcal{I}_1(\bar{\alpha}R)}\right|^2 \Big(|\hat{g}(1) + \hat{g}(-1) - \alpha_1|^2 + |i(\hat{g}(1) - \hat{g}(-1)) - \beta_1|^2\Big) \\ &\qquad + \left|\frac{\mathcal{I}_1(\bar{\alpha}R)}{\mathcal{I}_0(\bar{\alpha}R)}\right|^2 |\hat{g}(0) - \alpha_0|^2 + \sum_{|k|>1} \left|\frac{\mathcal{I}_{k-1} + \mathcal{I}_{k+1}}{2\mathcal{I}_k(\bar{\alpha}R)}\right|^2 |\hat{g}(k)|^2 \\ \leq &\left|\frac{\mathcal{I}_0 + \mathcal{I}_2}{2\mathcal{I}_1(\bar{\alpha}R)}\right|^2 \Bigg(|\hat{g}(1) + \hat{g}(-1) - \alpha_1|^2 + |i(\hat{g}(1) - \hat{g}(-1)) - \beta_1|^2 \\ &\qquad + \sum_{|k|>1} k^2\, |\hat{g}(k)|^2\Bigg) + \left|\frac{\mathcal{I}_1(\bar{\alpha}R)}{\mathcal{I}_0(\bar{\alpha}R)}\right|^2 |\hat{g}(0) - \alpha_0|^2, \end{aligned}$$

because standard properties of modified Bessel functions yield,

$$\forall (x > 0, n \in \mathbb{N}), \qquad \left|\frac{\mathcal{I}_{n-1} + \mathcal{I}_{n+1}}{2\mathcal{I}_n(x)}\right|^2 \leq n^2 \left|\frac{\mathcal{I}_0 + \mathcal{I}_2}{2\mathcal{I}_1(x)}\right|^2.$$

Each term can be bounded as follows:

– $|\hat{g}(0)-\alpha_0| = |(\hat{g}(0)-\mathbf{a}_0)+(\mathbf{a}_0-\alpha_0)| = |\hat{g}(0)-\mathbf{a}_0+\mathbf{a}_2|$;
– $|\hat{g}(1)+\hat{g}(-1)-\alpha_1| = |\hat{g}(1)+\hat{g}(-1)-\mathbf{a}_1+2\mathbf{a}_2|$;
– $|i(\hat{g}(1)-\hat{g}(-1))-\beta_1| = |i(\hat{g}(1)-\hat{g}(-1))-\mathbf{b}_1|$;
– $\sum_{|k|>1} k^2\,|\hat{g}(k)|^2 \leq \|g\|^2_{H^1}$.

Since g is real-valued and $\mathbf{a}_0, \mathbf{a}_1, \mathbf{b}_1, \mathbf{a}_2$ are computed by trapezoidal rule with $N=4$, we use triangular inequalities in conjunction with Lemma 5,

$$\mathbf{a}_0 - \hat{g}(0) = \sum_{k\in\mathbb{Z}^*} \hat{g}(4k), \qquad \mathbf{a}_2 = 4\Re(\hat{g}(2)) + 2\sum_{k\neq\{0,-1\}} \Re\big(\hat{g}(2+4k)\big),$$

$$\mathbf{a}_1 - 2\Re(\hat{g}(1)) = 2\Re(\hat{g}(3)) + 2\Re(\hat{g}(5)) + \sum_{|k|>1} \hat{g}(1+4k) + \hat{g}(-1+4k),$$

$$\mathbf{b}_1 - 2\Im(\hat{g}(1)) = 2\Im(\hat{g}(3)) + 2\Im(\hat{g}(5)) - i\sum_{|k|>1} \hat{g}(1+4k) - \hat{g}(-1+4k),$$

so that there is no error if $\hat{g}(k)=0$ when $|k|\geq 2$.

□

Theorem 4.1 expresses the fact that, while being only endowed with a 5-points stencil, the "Steklov scheme" (4.11) delivers a high accuracy if the exact solution is smooth, hence contains mostly low frequencies. Such regularity in a square domain requires smooth boundary data to be supplemented by compatibility conditions (A.2) at each corner, in order to apply Theorem A.2. This is a situation closely related to "well-balanced methods" in 1D, see also [3, 16, 19] for 2D considerations. In particular, the modified Bessel functions contained in (4.11), which numerically allow not to split between the Laplacian and the zero-order term, moreover can fit the sharp layers appearing in the solution in case the potential becomes stiff (like "exponential-fit" methods in 1D). However, our error bound doesn't directly extend to

$$-\Delta u + \alpha^2\, u = f(x,y), \qquad u\Big|_{\partial\Omega} = g,$$

because the 2D scheme approximates the source f as a piecewise constant function inside each disk $D_R(i-\frac{1}{2}, j-\frac{1}{2})$ (see [17, page 177]); see *e.g.* [4] for more details. Moreover, "compatibility conditions" involving f would be more intricate, see [2, 24].

5. Two-dimensional numerical illustrations.

5.1. Validation of error estimates. To assess practically the former estimates, the following exact solutions were considered in $\Omega = (-1,1)^2$ with $\varepsilon = 0.75$,

$$\mathcal{E}_0(x,y) = \mathcal{I}_0(r/\varepsilon), \quad r^2 = x^2+y^2, \quad \tan\theta = y/x,$$
$$\mathcal{E}_1(x,y) = -\mathcal{E}_0(x,y) + \mathcal{I}_1(r/\varepsilon)\,(\cos\theta - 0.5\sin\theta)$$
$$\mathcal{E}_2(x,y) = 2\mathcal{E}_1(x,y) + 0.5\,\mathcal{I}_2(r/\varepsilon)(\sin 2\theta + \cos 2\theta).$$

These exact solutions to $-\varepsilon^2\Delta u + u = 0$ allow to check both the accuracy of (4.11) and the numerical features of a computational domain endowed with "corners". Indeed, boundary data of $\mathcal{E}_0, \mathcal{E}_1, \mathcal{E}_2$ on $\partial\Omega$ display Lipschitz areas, where "compatibility conditions" (see Appendix A) aren't satisfied and most of the pointwise errors of the Steklov scheme accumulates: this is easily noticed with the radial solution $\mathcal{E}_0$. On the right column of Fig. 5.1, the convergence rates of standard finite-differences, discrete weighted means (DWM, see [15, 23, 52]) and (4.11) are compared. The red line, which indicates second-order accuracy, allows to easily check that both finite-differences and

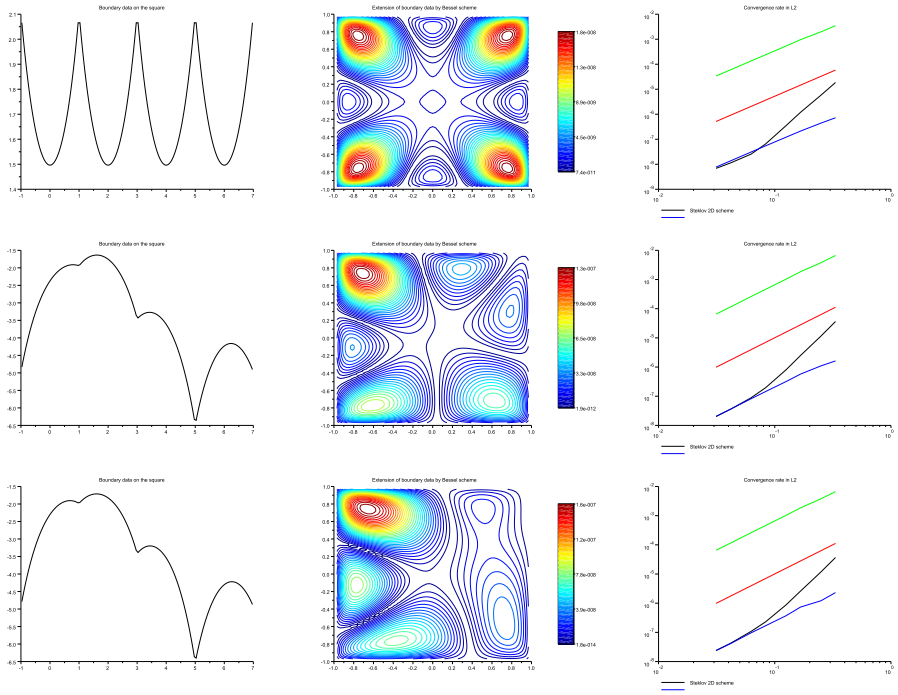

FIGURE 5.1. *Boundary data (left), pointwise errors (middle) and L^2 convergence rates (right) for finite-differences, discrete weighted-means and Steklov schemes. Red line indicates second order.*

DWM are second-order methods, the size of the errors being very different, though. The Steklov scheme (4.11) behaves differently, in the sense that when the grid is coarse, it displays a fourth-order accuracy, which degrades to second-order when $\Delta x/\varepsilon$ goes below a certain value. This was to be expected as the modified Bessel functions behave like polynomials when their argument is very small (see also [52]). The DWM (or "tailored", [23, 25]) methods, while being very accurate on $\mathcal{E}_0, \mathcal{E}_1, \mathcal{E}_2$, aren't endowed with such a fast convergence property. Next, in order to illustrate the behavior for smaller ε's, another (more complex) exact solution,

$$\mathcal{E}_3(x,y) = 0.5\,\mathcal{I}_2(r/\varepsilon)(\sin 2\theta + \cos 2\theta) + \mathcal{I}_3(r/\varepsilon)\sin 3\theta, \qquad \varepsilon = 0.1125 \text{ or } 0.075,$$

was computed by both the DWM and Steklov schemes; see Fig. 5.2. By inspecting boundary data, one sees that a seemingly small variation in ε can produce a strong increase of the "spikes" at the $\Omega = (-1,1)^2$ square's corners where compatibility conditions aren't met. Indeed, for smaller ε, most of the numerical error accumulates in these regions. Both numerical methods appear to be similar and to converge at second order in L^2 when $\Delta x/\varepsilon$ is moderate; when $\Delta x/\varepsilon$ is bigger, the Steklov scheme seems to behave a little bit better than the DWM (see Fig. 5.2, bottom).

5.2. Simple harmonic potential. Consider now an eigenvalue problem like,

$$-\varepsilon^2 \Delta u + V(x,y)u = \lambda u, \qquad (x,y) \in \mathbb{R}^2,$$

for which both eigenvalues λ's and eigenfunctions are explicitly known when posed in the whole space, see Theorem 2.1. When $0 < \varepsilon$ is small enough, this explicit spectrum

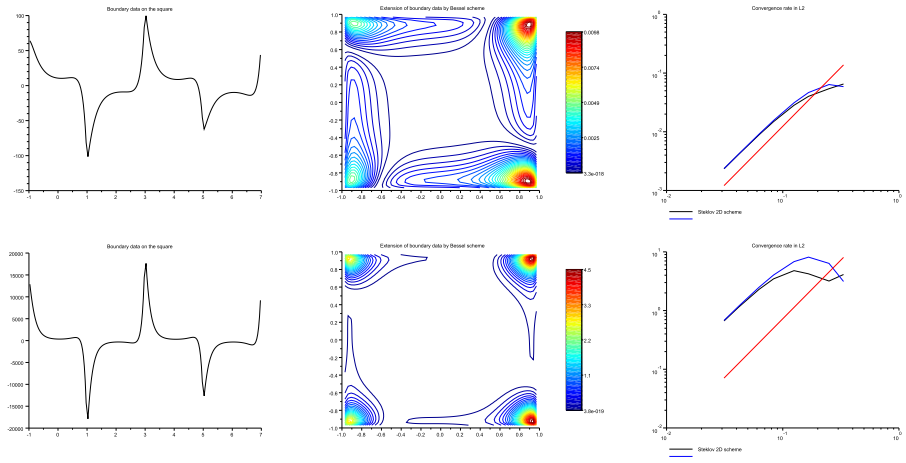

FIGURE 5.2. *Boundary data (left), pointwise errors (middle) and L^2 convergence rates (right) for Tailored (discrete weighted-means) and Steklov schemes. Red line again indicates second order.*

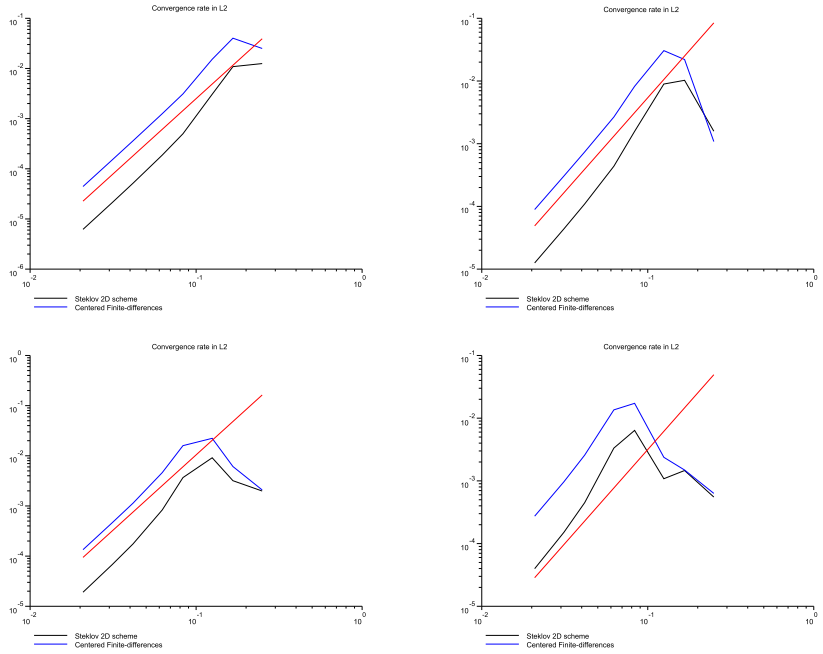

FIGURE 5.3. *Decay of L^2 norm (4.16): $\varepsilon = 0.0066$ (top, left), $\varepsilon = 0.0033$ (top, right), $\varepsilon = 0.0022$ (bottom, left) and $\varepsilon = 0.0011$ (bottom, right), for problem (5.1). Red line indicates third order.*

can still be used in order to quantify pointwise errors of numerical schemes, even if the computational domain must be restricted to a bounded square in $\mathbb{R}^2$. Accordingly,

$$-\varepsilon^2 \Delta u + V(x,y)u = \lambda u, \qquad V(x,y) = 0.25\left(|x-0.5|^2 + |y-0.5|^2\right), \tag{5.1}$$

is now posed in $x, y \in (0,1)^2$ and its numerical spectrum is sought by both centered finite-differences, and the "Steklov 2D scheme". The Gaussian ground-state ϕ_0^ε allows

to measure practically the decay of L^2 norms (4.16) as $\Delta x \to 0$ for both numerical algorithms: on Fig. 5.3, errors appear to decay at an order higher than 3 as soon as $\Delta x/\varepsilon$ is small enough, so that the grid can efficiently represent the numerical approximation. The decay corresponding to third order is illustrated by a red line on Fig. 5.3. To minimize the influence of truncating the computational domain without restricting too much the support of eigenfunctions, a convenient value of ε was experimentally found to be $\varepsilon \simeq 0.007$, with a grid 32×32. Pointwise relative errors are displayed on Fig. 5.4: the left column displays relative errors coming from the "Steklov scheme" which suffer from less "mesh imprinting" (and are smaller) than the ones generated by standard centered finite differences (on the right column).

REMARK 3. *An inspection of Fig. 5.3 suggests that there are three different regimes (instead of apparently two for finite differences) for the "Steklov scheme":*

- *a stiff one, $\varepsilon \ll \Delta x$, where the grid is really too coarse for a radial solution,*
- *an intermediate one for which $\varepsilon \simeq \Delta x$ where L^2 errors can decay very fast (faster than order 4) compared to centered finite-differences,*
- *a fine-grid one, $\varepsilon \gg \Delta x$ for which L^2 errors decay at a rate close to order 3.*

5.3. (A-)symmetric two-well potential. We illustrate this case with the "Steklov 2D scheme" on the same computational grid, $\varepsilon = 0.02$ and the potentials,

$$\begin{aligned} V(x,y) &= 1.01 - \exp\Big(-30\big(|x-0.65|^2+|y-0.35|^2\big)\Big) \\ &\qquad - \exp\Big(-30\big(|x-0.35|^2+|y-0.65|^2\big)\Big), \\ (V+\delta V)(x,y) &= 1.01 - \exp\Big(-30.5\big(|x-0.65|^2+|y-0.35|^2\big)\Big) \\ &\qquad - \exp\Big(-30\big(|x-0.35|^2+|y-0.65|^2\big)\Big), \end{aligned}$$

which share the same depth, but one is slightly wider than the other. On the left column of Fig. 5.5, usual symmetric eigenfunctions are generated by the scheme in presence of the double-Gaussian potential $V(x,y)$, $x,y \in (0,1)^2$ with Dirichlet boundaries and $2^5 \times 2^5$ grid points. As expected, the ground state has a definite sign, in accordance with the statements in Proposition 2. For the perturbed potential $V+\delta V$, a quite different picture emerges as the perturbed ground state is now strongly localized in the largest well, still being of a definite sign. The first perturbed excited state is localized in the narrow well and is endowed with small negative values. More excited eigenfunctions are less localized, but still, are never symmetric. Discrete orthogonality is checked in practice by looking at the L^2 scalar products: it was found to hold, up to machine accuracy ($\simeq 10^{-16}$) for both the five first unperturbed eigenfunctions, and the perturbed ones (see also [37] for other benchmarks).

5.4. Time-dependent problem with two asymmetric wells. The 2D Steklov scheme (4.11) can be recast as a time-marching algorithm, see [17, page 184], for

$$\partial_t u + \varepsilon^2 \Delta u + V(x,y)u = 0. \qquad (x,y) \in (0,1)^2, \tag{5.2}$$

with Dirichlet boundary conditions. The potential was chosen as,

$$\begin{aligned} V(x,y) \;=\; & 0.95 - \exp\Big(-10\big(|x-0.75|^2+|y-0.25|^2\big)\Big) \\ & - \exp\Big(-25\big(|x-0.25|^2+|y-0.75|^2\big)\Big). \end{aligned} \tag{5.3}$$

Numerical results for $\varepsilon^2 = 0.00005$, with a 32×32 grid, and Gaussian initial data are

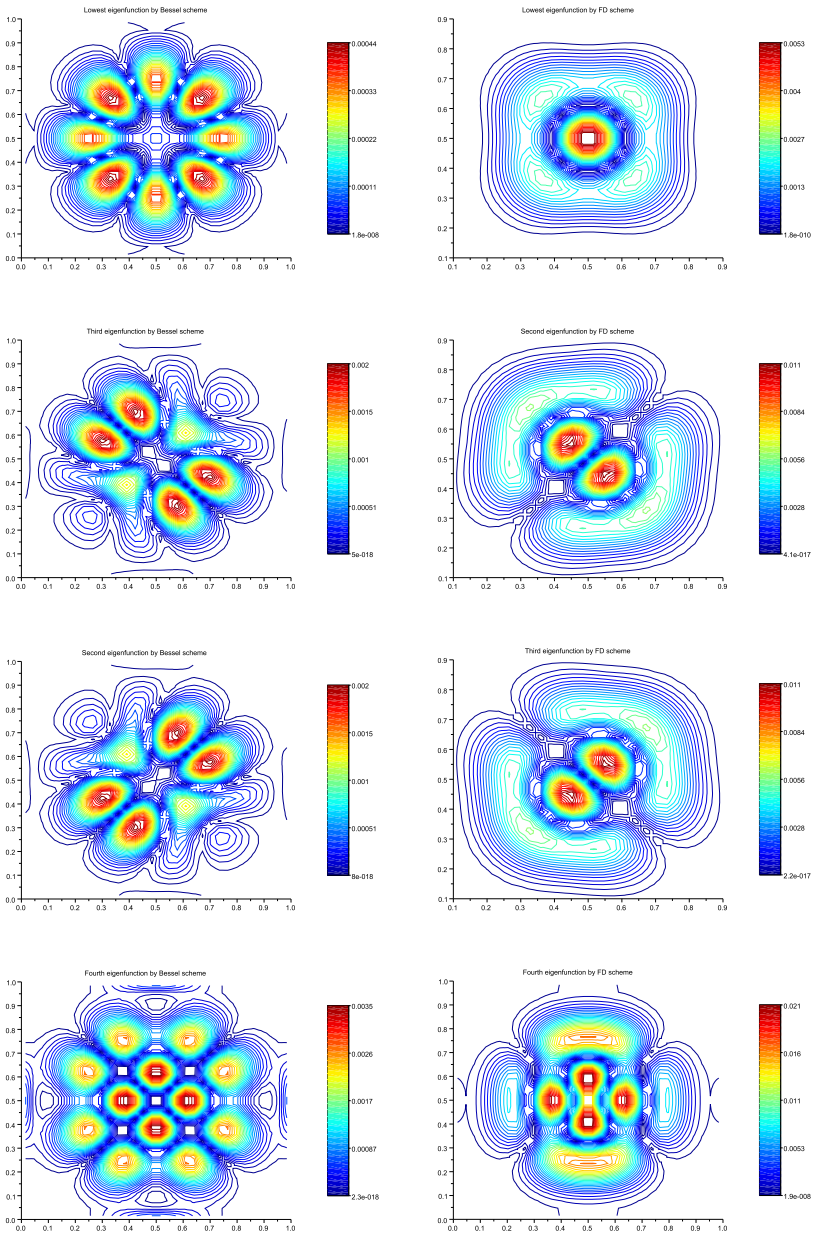

FIGURE 5.4. *Steklov scheme with Bessel functions (left) vs. centered FD (right).*

displayed on Fig. 5.6. As expected from the spectral results derived in Section 3, the numerical solution accumulates more and more in the widest well, in agreement with the shape of the ground-state for asymmetric potentials, as displayed (for instance) on the right column of Fig. 5.5. The large-time behavior of (5.3) sees all the initial data's mass accumulate in the widest well, the narrow one being depleted (at a rate which slows down as time grows). This is what is illustrated on the bottom line of

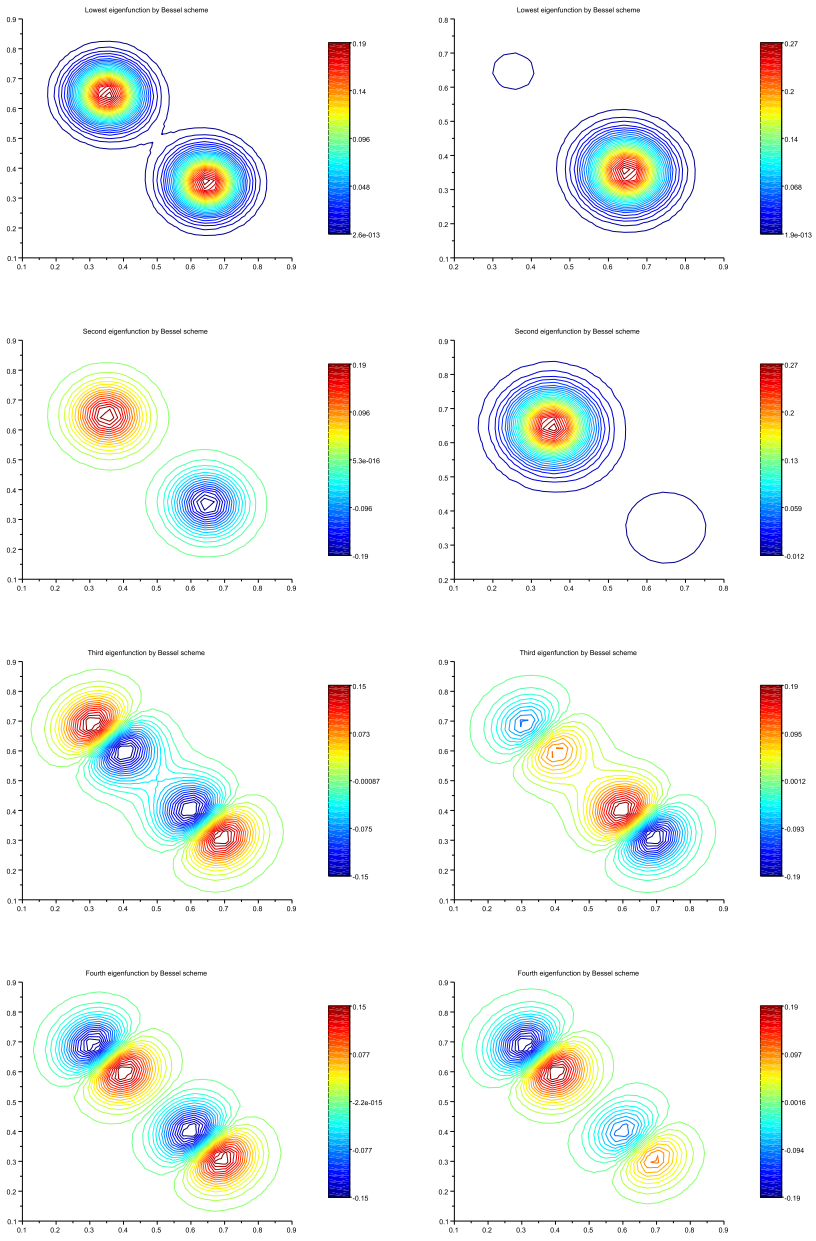

FIGURE 5.5. *Steklov scheme: symmetric (left) vs. asymmetric (right) potential.*

Fig. 5.6, where the numerical steady-state is shown to have nearly all its mass inside the widest well. Beyond $T \simeq 50$, the rate of change is very slow, though.

6. Conclusion and outlook. After recalling B. Simon's "flea on the elephant" phenomenon in 1D, see Fig. 1.1, analytical bounds were derived in Section 3 dealing with various perturbations of the classical quadratic harmonic potential; in particular,

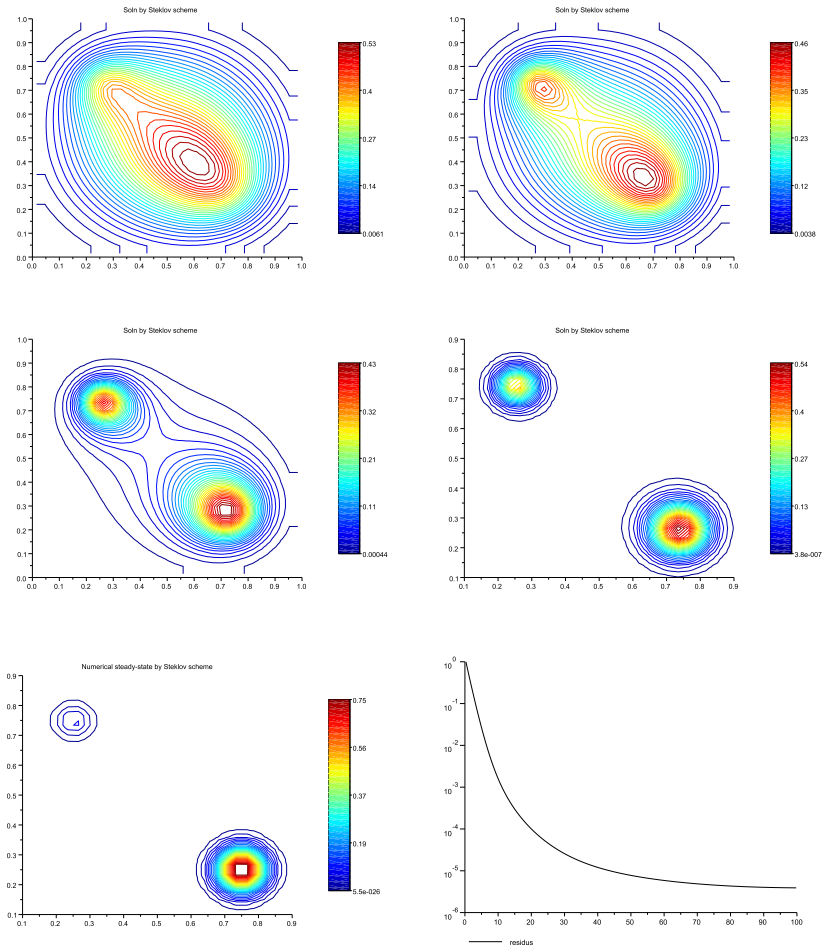

FIGURE 5.6. *Numerical solutions of time-dependent problem (5.2)–(5.3) at times* $T = 2, 3, 7, 20$*; numerical steady-state at* $T = 100$ *(bottom, left) and corresponding* L^2 *residues (bottom, right).*

mass-accumulation in wider wells was justified with elementary arguments (see also [9, 20, 31, 45]). Then, in Section 4, the 2D scheme of [16, 17] is derived in a way which allows to produce error bounds for the constant coefficient case (see [52]). Such an algorithm, involving modified Bessel functions in 2D, is reminiscent of "discrete weighted means", see [15, 23, 25, 40, 52]. Accordingly, the expected localization behavior is retrieved in Section 5, mostly for rough computational grids for which $\varepsilon/\Delta x \ll 1$, see also [51], in both static and time-dependent contexts. As an outlook, we outline an extension to a fourth-order Cahn-Hilliard [5, 12] type of equation:

$$\partial_t u - \Delta\Big(u(1-u^2) - \varepsilon\Delta u\Big) = 0, \qquad x, y \in (0,1)^2. \tag{6.1}$$

Following [50], we recast it as a system, except that, here, the nonlinearity is handled as a (locally) constant coefficient, (*i.e.* mass-conservation property may be lost)

$$\partial_t u + \varepsilon\Delta v - \alpha^2\, v = 0, \qquad v = \Delta u, \qquad \Delta\big(u(1-u^2)\big) \simeq (1-\bar{u}^2)\Delta u.$$

The "frozen parameter" α varies from disk to disk (see Fig. 4.1),

$$\alpha^2(t^n, x_{i\pm\frac{1}{2}}, y_{j\pm\frac{1}{2}}) = 1 - u^2(t^n, x_{i\pm\frac{1}{2}}, y_{j\pm\frac{1}{2}}).$$

Starting from random initial data belonging to the interval $(-1, 1)$, and fixing $\varepsilon =$

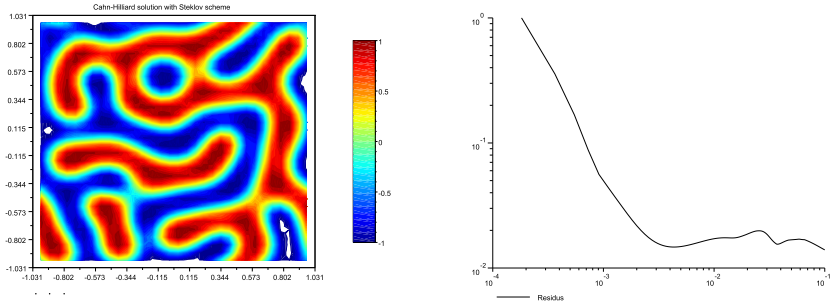

FIGURE 6.1. *Simulation of Cahn-Hilliard equation (6.1): steady-state (left) and residues (right).*

0.002 with a 32×32 computational grid, the expected phase-separation phenomenon, displayed on Fig. 6.1, was retrieved by using an explicit Euler time-integrator.

Acknowledgments. Enrique Zuazua's research was supported by the Advanced Grant DyCon (Dynamical Control) of the European Research Council Executive Agency (ERC), the MTM2014-52347 and MTM2017-92996 Grants of the MINECO (Spain) and the ICON project of the French ANR-16-ACHN-0014. L.G. thanks Profs. François Bouchut and Roberto Natalini for some technical discussions.

Appendix A. Elliptic regularity in a planar, square domain.

Let $\Omega = (0, 1) \times (0, 1)$ be the (open) unit square and Γ stand for its boundary. Consider the following strictly elliptic operator in Ω,

$$\mathcal{L}[u] = -\Delta u + r(x, y)u = 0, \qquad u\Big|_\Gamma = g, \qquad r \geq 0, \tag{A.1}$$

where both r and g are smooth functions. Because the domain is convex, but endowed with "corners", the variational solution to (A.1) cannot be expected to be smoother than H^2 in general, see [21] and, *e.g.*, [29, Theorem 4.3]. Refined regularity estimates relying on Besov spaces theory were given in [8, Carollary 3.1]:

THEOREM A.1. *Let $r \equiv 0$ in (A.1), which reduces to Laplace's equation, and $g \in W^{s,p}(\Gamma)$ with $p < \frac{2}{1-\varepsilon}$ and $s \in (1 - \varepsilon, 1)$: the harmonic solution $u \in W^{t,q}(\Omega)$ for*

$$\frac{1}{2+s} < q \leq p, \qquad 0 < t < s + \frac{1}{q}.$$

If $g \in H^1(\Gamma)$, then $s = 1, p = 2$ and $u \in W^{t,q}(\Omega)$ with $\frac{1}{3} < q \leq 2$ and $0 < t < 1 + \frac{1}{q}$.

Another point of view consists in seeking under which restrictions on g the solution u can be as smooth as if (A.1) was solved in a smooth domain. Following [33], let

$$u(x, y) = \sum_{j,\ell=0}^{3} \Lambda_j^\ell(g)\phi_{i,j}(x, y) + v(x, y), \qquad v \text{ smooth},$$

where $\ell = 0,1,2,3$ is the index of a vertex, and Λ stands for a linear functional acting on singular profiles ϕ localized around each corner of the domain Ω. These functional are linear combinations of differential operators acting on g, and the number of involved derivatives of g increases with respect to the index k. Accordingly, such a decomposition suggests that cancelling the Λ's should ensure that u can become as smooth as its remainder v. These functionals were studied in many papers, after early works by Nicol'ski, Volkov, Fufaev, see [34, Chap. III]: for (A.1) and $x = y = 0$,

$$\Lambda_j(g) = \frac{d^{2j}g}{dx^{2j}}(0^+,0) - (-1)^j \frac{d^{2j}g}{dy^{2j}}(0,0^+) \qquad (A.2)$$
$$- \sum_{i=1}^{j} (-1)^{i-1} \frac{\partial^{2(j-i)}}{\partial x^{2(j-i)}} \frac{\partial^{2(j-i)}}{\partial y^{2(i-1)}} \big(r(0,0)u(0,0)\big), \qquad j = 0,1,2,...$$

Following [6, eq. (2.1)], see also [1, eq. (1.8-9)], the first ones in $x = y = 0$ are:

$$\Lambda_0(g) = g(0^+,0) - g(0,0^+),$$
$$\Lambda_1(g) = \frac{d^2g}{dx^2}(0^+,0) + \frac{d^2g}{dy^2}(0,0^+) - r(0,0)u(0,0),$$
$$\Lambda_2(g) = \frac{d^4g}{dx^4}(0^+,0) - \frac{d^4g}{dy^4}(0,0^+) + \left(\frac{\partial^2}{\partial x^2} - \frac{\partial^2}{\partial y^2}\right)\big(r(0,0)u(0,0)\big).$$

If all the derivatives of both g and r vanish close to each corner, (A.2) holds. According to [24, Theorem 3.2] (see also [2, Theorem 2] and references therein), these "compatibility conditions" suffice for (A.1) to pass the Hölder regularity of g onto u:

THEOREM A.2. *Let $g \in C^{2,\lambda}$ on Γ minus its 4 vertices and $\Lambda_0^\ell(g) = 0$ for $\ell = 0,1,2,3$: the solution of (A.1) $u \in C^{2,\lambda}(\bar\Omega)$. Moreover, for $\bar\Omega = [0,1]\times[0,1]$,*

$$\boxed{u \in C^{2k,\lambda}(\bar\Omega) \Leftrightarrow g \in C^{2k,\lambda} \text{ and } \Lambda_j^\ell(g) = 0 \text{ for } j \le k \text{ and } \ell = 0,1,2,3,}$$

and if, under the same conditions, $g \in C^{2k+1,\lambda}$, then $u \in C^{2k+1,\lambda}(\bar\Omega)$.

Such regularity results can be formulated in other functional spaces, see for instance [35, 36]. There are several variants of this statement, like in [1, 10, 28, 33]:

COROLLARY 1. *Assume that $g \in C^{1,1}$ on Γ minus its 4 vertices and $\Lambda_0^\ell(g) = 0$ for $\ell = 0,1,2,3$, then the following second derivatives of u are bounded in Ω,*

$$\max\left(\left|\frac{\partial^2 u}{\partial x^2}\right|, \left|\frac{\partial^2 u}{\partial y^2}\right|\right) \le C, \quad \textit{but not the mixed one,} \quad \frac{\partial^2 u}{\partial x\,\partial y}.$$

Restricting (A.2) to $k = 0$ only brings $g(0^+,0) = g(0,0^+)$ at the vertex $x = y = 0$, so that condition $\Lambda_0^\ell(g) = 0$ means that g is continuous at all four vertices of Ω.

Appendix B. Trapezoidal rule and circular traces.

Let γ_R be the "circular trace operator" $H^s(\mathbb{R}^2) \to H^{s-\frac12}(0, 2\pi R)$ for which,

$$\gamma_R : u \mapsto \gamma_R[u], \qquad \gamma_R[u](\theta) = u(R\cos\theta, R\sin\theta), \qquad f(x) = \gamma_R[u](R\theta),$$

where $\theta \in (0, 2\pi)$. The proof of Lemma 5 is split into several steps:

- Being $f : (0, T = 2\pi R) \to \mathbb{R}$ periodic, it rewrites as a Fourier series,

$$f(x) = \sum_{k\in\mathbb{Z}} \hat f(k) \exp(ik\frac{2\pi x}{T}), \qquad \hat f(k) = \frac{1}{T}\int_0^T f(x)\exp(-ik\frac{2\pi x}{T})\mathrm{d}x.$$

Accordingly, the N-points (Nyström's) "method of rectangles" rewrites:

$$\frac{T}{N}\sum_{j=0}^{N-1} f(j\frac{T}{N}) = \frac{T}{N}\sum_{j=0}^{N-1}\left(\sum_{k\in\mathbb{Z}}\hat{f}(k)\exp(ik\frac{2\pi j}{N})\right)$$
$$= \frac{T}{N}\sum_{k\in\mathbb{Z}}\hat{f}(k)\left(\sum_{j=0}^{N-1}\exp(ik\frac{2\pi j}{N})\right).$$

- An elementary observation is that

$$\frac{1}{T}\int_0^T \exp(ik\frac{2\pi x}{T})\mathrm{d}x - \frac{1}{N}\sum_{j=0}^{N-1}\exp(ik\frac{2\pi j}{N}) = -\chi(k\in N\mathbb{Z}_*),$$

where χ stands for the indicator function and $\mathbb{Z}_*$, for $\mathbb{Z}$ without 0. Indeed, for $k\in\mathbb{Z}$, being a geometric summation of reason $\exp(ik\frac{2\pi}{N})$,

$$\sum_{j=0}^{N-1}\exp(ik\frac{2\pi j}{N}) = \frac{1-\exp(ik\,2\pi)}{1-\exp(ik\frac{2\pi}{N})} = N\,\chi(k\in N\mathbb{Z}),$$

so the numerator always vanishes. Indexes $k\in N\mathbb{Z}$ are such that the denominator cancels, too: a Taylor expansion yields the expected result. Yet,

$$\hat{f}(0) - \left(\frac{1}{N}\sum_{k\in\mathbb{Z}}\hat{f}(k)\sum_{j=0}^{N-1}\exp(ik\frac{2\pi j}{N})\right) = -\sum_{k\in\mathbb{Z},\,k\neq 0}\hat{f}(Nk), \tag{B.1}$$

and it remains to estimate the lacunary sum on the right-hand side.

- To estimate the right-hand side of (B.1), we recall that f is the restriction on a circle of radius $R>0$ and centered in (x_0,y_0) of $u(x,y)\in H^s(\mathbb{R}^2)$. Standard trace theory [41] gives that $f\in H^{s-\frac{1}{2}}(0,T)$: if $s>1$, Sobolev inequalities ensure that f is continuous. Moreover, for any index $k\in\mathbb{N}$,

$$\begin{aligned}
\hat{f}(k) &= \frac{1}{2\pi}\int_0^{2\pi} u(R\cos\theta, R\sin\theta)\exp(-ik\theta)\mathrm{d}\theta\\
&= -\frac{R}{2\pi}\int_0^{2\pi}\Big(-\sin\theta\,\partial_x u + \cos\theta\,\partial_y u\Big)\left(\frac{-1}{ik}\exp(-ik\theta)\right)\mathrm{d}\theta\\
&= \frac{-iR}{2\pi k}\int_0^{2\pi} -\partial_x u\Big(\sin\theta\,\exp(-ik\theta)\Big) + \partial_y u\Big(\cos\theta\,\exp(-ik\theta)\Big)\mathrm{d}\theta\\
&= \frac{R}{4\pi k}\int_0^{2\pi}\partial_x u\Big(\exp(-i(k-1)\theta) - \exp(-i(k+1)\theta)\Big)\mathrm{d}\theta\\
&\qquad - \frac{iR}{4\pi k}\int_0^{2\pi}\partial_y u\Big(\exp(-i(k-1)\theta) + \exp(-i(k+1)\theta)\Big)\mathrm{d}\theta.
\end{aligned}$$

Recalling that $\gamma_R[u](\theta) = u(R\cos\theta, R\sin\theta)$, this yields:

$$\widehat{\gamma_R[u]}(k) = \frac{R}{2k}\Big(\widehat{\gamma_R[\partial_x u]}(k-1) - \widehat{\gamma_R[\partial_x u]}(k+1)$$
$$-i\big(\widehat{\gamma_R[\partial_y u]}(k-1) + \widehat{\gamma_R[\partial_y u]}(k+1)\big)\Big),$$

so that, the smoothness of u induces Fourier coefficients of $\gamma_R[u]$ which are of the order of powers of R, the radius of the circle. By induction, this calculation can be repeated until,

- either Fourier coefficients of index zero are reached, and integrating by parts isn't possible;
- or the function u hasn't enough regularity (when $|k| > s - \frac{1}{2}$).

Finally, we get an estimate on the size of Fourier coefficients on the circle of radius R, which can obviously be used to control the error (B.1):

$$\boxed{\forall k \in \mathbb{Z}, \qquad \left|\widehat{\gamma_R[u]}(k)\right| = O\left(R^{\min(|k|, s-\frac{1}{2})}\right).} \tag{B.2}$$

If $s - \frac{1}{2} \geq |k|$, then in general,

$$\forall k \in \mathbb{Z}, \qquad \left|\widehat{\gamma_R[u]}(k)\right| = O(R^{|k|}) \left|\widehat{\gamma_R[D^{|k|}u]}(0)\right|,$$

which is the "circular average" of $D^{|k|}u$, and the value at the circle's center of its harmonic extension. This agrees with the approximate values found at §4.2.

REFERENCES

[1] V.B. Andreev, *On the Accuracy of Grid Approximations to Nonsmooth Solutions of a Singularly Perturbed Reaction–Diffusion Equation in the Square*, Differ. Equations 42 (2006) 954–966.

[2] A. Azzam, *On Differentiability Properties of Solutions of Elliptic Differential Equations*, J. Math. Anal. Applic. 75 (1980) 431–440.

[3] R. Bianchini, L. Gosse, *A truly two-dimensional discretization of drift-diffusion equations on Cartesian grids*, SIAM J. Numer. Anal. 56 (2018) 2845–2870.

[4] G. Birkhoff, S. Gulati, *Optimal few points discretizations of linear source problems*, SIAM J. Numer. Anal. 11 (1974) 700–728.

[5] J.W. Cahn, J.E. Hilliard, *Free energy of a nonuniform system. I. Interfacial free energy*, J. Chem. Phys. 28 (1958): 258.

[6] C. Clavero, J.L. Gracia, E. O'Riordan, *A parameter robust numerical method for a two dimensional reaction-diffusion problem*, Math. Comput. 74 (2005) 1743–1758.

[7] E.N. Dancer, J. Lopez-Gomez, *Semiclassical analysis of general second order elliptic operators on bounded domains*, Trans. Amer. Math. Soc. 352 (2000) 3723–3742.

[8] S. Dahlke, R.A. Devore, *Besov regularity for elliptic boundary value problems*, Comm. P.D.E. 22 (1997) 1–16.

[9] T. Dauphine, F. Marsiglio, *Asymmetric wave functions from tiny perturbations*, American J. Phys. 83 (2015): 861.

[10] A.A. Dosiyev, *New Properties of 9-Point Finite Difference Solution of the Laplace Equation*, Mediterr. J. Math. 8 (2011), 451–462.

[11] P.C. DuChateau, D.W. Zachmann, **Schaum's Outline of Partial Differential Equations**, McGraw-Hill, New York, 1986.

[12] C. M. Elliott, D.A. French, *Numerical Studies of the Cahn-Hilliard Equation for Phase Separation*, IMA J. Applied Math. 38 (1987) 97–128.

[13] M. Escobedo, O. Kavian, *Variational problems related to self-similar solutions of the heat equation*, Nonlinear Anal.: Theory, Meth. & Applic. 10 (11) (1987), 1103-1133.

[14] M. Filoche, S. Mayaboroda, B. Patterson. *Localization of eigenfunctions of a one-dimensional elliptic operator*, in Contemporary Mathematics 581 (2012): 99-116.

[15] E.C. Gartland Jr., *Discrete weighted mean approximation of a model convection-diffusion equation*, SIAM J. Sci. Stat. Comp. 3 (1982) 460–472.

[16] L. Gosse, *Dirichlet-to-Neumann mappings and finite-differences for anisotropic diffusion*, Comput. & Fluids 156 (2017) 58–65.

[17] L. Gosse, *Viscous equations treated with $\mathcal{L}$-splines and Steklov-Poincaré operator in two dimensions*, in **Innovative Algorithms & Analysis**, DOI: 10.1007/978-3-319-49262-9_6.

[18] L. Gosse, *$\mathcal{L}$-Splines and Viscosity Limits for Well-Balanced Schemes Acting on Linear Parabolic Equations*, Acta Applic. Math. 153 (2018) 101–124.

[19] L. Gosse, *Aliasing and two-dimensional well-balanced for drift-diffusion equations on square grids*, preprint (2018).
[20] S. Graffi, V Grecchi, G Jona-Lasinio, *Tunnelling instability via perturbation theory*, J. Phys. A: Math. Gen. 17 (1984) 2935–2944
[21] P. Grisvard, **Elliptic problems in non smooth domains**, Pitman (1985).
[22] J. Gopalakrishnan, L. Grubišić, J. Ovall, *Filtered subspace iteration for selfadjoint operators*, preprint (2017).
[23] H. Han, Z. Huang, R. B. Kellogg, *A Tailored Finite Point Method for a Singular Perturbation Problem on an Unbounded Domain*, J Sci. Comput. (2008) 36: 243–261.
[24] H. Han, R. B. Kellogg, *Differentiability properties of solutions of the equation* $-\varepsilon^2\Delta u + ru = f(x, y)$ *in a square*, SIAM J. Math. Anal. 21(2) (1990) 394-408.
[25] H. Han, Z. Zhang, *Multiscale tailored finite point method for second order elliptic equations with rough or highly oscillatory coefficients*, Commun. Math. Sci. 10 (2012) 945–976.
[26] P. Harrison. **Quantum wells, wires and dots: theoretical and computational physics of semiconductor nano-structures**. John Wiley & Sons, 2005.
[27] B. Helffer, J. Sjostrand, *Multiple wells in semi-classical limit*, Comm. P.D.E. 9 (1984) 337-408.
[28] T. Hell, A. Ostermann, M. Sandbichler, *Modification of dimension-splitting methods–overcoming the order reduction due to corner singularities*, IMA J. Numer. Anal. 35 (2015) 1078–1091.
[29] D. Hua, *A regularity result for boundary value problems on Lipschitz domains*, Ann. Fac. Sci. Toulouse 10 (1989) 325–333.
[30] D. Holcman, I. Kupka, *Singular perturbation for the first eigenfunction and blow-up analysis*, Forum Math. **18** (2006), 445-518.
[31] V. Jelic, F. Marsiglio, *The double well potential in quantum mechanics: a simple, numerically exact formulation*, European J. Phys. 33 (2013) 33 (6), 1651.
[32] G. Jona-Lasinio, F. Martinelli, E. Scoppola, *New approach in the semiclassical limit of quantum mechanics*, Comm. Math. Phys. 80 (1981), 223-254.
[33] B. Kellogg, *Some Simple Boundary Value Problems with Corner Singularities and Boundary Layers*, Computers Math. Applic. 51 (2006) 783-792.
[34] V.A. Kondrat'ev, O.A. Oleinik, *Boundary-value problems for partial differential equations in non-smooth domains*, Russian Math. Surveys 38:2 (1983), 1–86.
[35] A. N. Konenkov, *The Dirichlet Problem in Zygmund Spaces in a Square*, Doklady Mathematics, 75 (2007) 16–19.
[36] A. N. Konenkov, *Dirichlet and Neumann problems for Laplace and heat equations in domains with right angles*, J. Math. Sciences. 150 (2008) 2507–2512.
[37] W. Kong, Z. Huang, *Asymptotic analysis and numerical method for singularly perturbed eigenvalue problems*, SIAM J. Scient. Comput. 40 A3293–A3321.
[38] N.P. Landsman, R. Reuvers, *A Flea on Schrödinger's Cat*, Found Phys 43 (2013) 373–407.
[39] A. Martinez, M. Rouleux, *Effet tunnel et puits dégénérés*, Comm. P.D.E. 13 (1988) 1157–1187.
[40] A. Mayo, *Fast High Order Accurate Solution of Laplace's Equation on Irregular Regions*, SIAM J. Sci. and Stat. Comput., 6 (1985) 144–157.
[41] Y. Miyazaki, *Sobolev Trace Theorem and the Dirichlet Problem in the Unit Disk*, Milan J. Math. 82 (2014) 297–312.
[42] J. Ralston, *Approximate eigenfunctions of the Laplacian*, J. Differ. Geom. 12 (1977) 87–100.
[43] J. Ralston, *On the construction of quasi-modes associated with stable periodic orbits*, Commun. Math. Phys. 51 (1976) 219–242.
[44] C.A. Reyes, G. Sweers, *An asymptotic eigenvalue problem for a Schrödinger type equation on domains with boundaries*, Rev Mat Complut (2016) 29:497–510.
[45] M. Selg, *Exactly solvable asymmetric double-well potentials*, Physica Skripta 62 (2000) 108–116.
[46] B. Simon, *Instantons, double wells and large deviations*, Bull. Amer. Math. Soc., 8 (1983).
[47] B. Simon, *Semiclassical Analysis of Low Lying Eigenvalues, II. Tunneling*, Ann. of Math. 1 (Vol. 120) (1984), 89-118.
[48] B. Simon, *Semiclassical analysis of low lying eigenvalues. IV. The flea on the elephant*, J. Funct. Anal. 63 (1) (1985), 123-136.
[49] Dae-Yup Song, *Tunneling and energy splitting in an asymmetric double-well potential*, Annals of Physics 323 (2008) 2991–2999.
[50] Z.-Z. Sun, *A second-order accurate linearized difference scheme for the two-dimensional Cahn-Hilliard equation*, Math. Comput. 64 (1995) 1463–1471.
[51] L. N. Trefethen, T. Betcke, *Computed eigenmodes of planar regions*, Contemporary Mathematics, 412 (2006), 297-314.
[52] J.B.R. do Val, M.G. Andrade, *On mean value solutions for the Helmholtz equation on square grids*, Appl. Num. Math. 41 (2002), 459-479.